ALMA MATER STUDIORUM - UNIVERSITÀ DI BOLOGNA

CAMPUS DI CESENA

DIPARTIMENTO DI INGEGNERIA DELL'ENERGIA ELETTRICA E DELL'INFORMAZIONE "GUGLIELMO MARCONI"

CORSO DI LAUREA MAGISTRALE IN INGEGNERIA BIOMEDICA

AN *IN SILICO* METHOD TO EVALUATE BONE REMODELLING AFTER TOTAL HIP ARTHROPLASTY IN A SIX YEARS LONGITUDINAL STUDY

Tesi in

Meccanica dei Tessuti Biologici LM

Relatore:
Prof. Luca Cristofolini

Presentata da:
Valentina Betti

Correlatori:
Prof. Paolo Gargiulo
Prof. Magnús Kjartan Gíslason

Sessione III
Anno Accademico 2019/2020

"There is a driving force more powerful than steam, electricity and atomic energy: the will".

Albert Einstein

Abstract

Total Hip Arthroplasty (THA) is generally considered to be one of the most successful orthopedic surgical procedures. The choice of the implant (cemented/uncemented) affects the bone remodelling around the prosthesis, along with other factors such as age, sex and level of physical activity. The aim of the study was to quantitatively evaluate how much these parameters affect the remodeling process and to locate where the changes occurred.
In this work, an *in silico* method was developed to assess the BMD variations of the proximal part of the femur one year and six years post-operatively. The differences in mineral density were also evaluated separately in the seven standard Gruen zones (GZ). Furthermore, a protocol was developed to evaluate where bony formations/resorptions were to occur. The method was then applied to process ten patients' data to verify its feasibility and repeatability.
A general trend was observed in the patients examined in this study, with an increase in percentage for the spongeous bone (particularly in GZ 3 and 5) and a decrease for the cortical one six years after THA (particularly in GZ 1, 2, 6, and 7). For the cemented group, a loss in density was observed in GZ 2, 3, and 6. For the uncemented group, the loss was localised only in GZ 1. Moreover, results from new bone formations shows that a bone resorption occurred in the proximal area of the femur one year post-operation.
Through the addition of a larger amount of data, this methodology will provide a tool to draw conclusions regarding BMD changes over the years and where these variations are more precisely localised in the femur. Such analysis will be supplied to surgeons in order to develop new strategies not merely regarding the selection of the optimal implant, but also concerning the best approach to rehabilitation and adjoining pharmacological therapy.

Abstract

L'intervento di artroplastica totale d'anca è considerato una delle procedure chirurgiche ortopediche con le più alte percentuali di successo. La scelta dell'impianto (cementato/non cementato) influisce sul rimodellamento osseo attorno alla protesi, insieme ad altri fattori come età, sesso e livello di attività fisica. Obiettivo dello studio è quello di valutare quantitativamente l'impatto di questi parametri sia dal punto di vista del processo fisiologico di rimodellamento osseo, che della localizzazione spaziale della variazione della densità minerale ossea nel segmento di riferimento.
In questo lavoro, è stato sviluppato un metodo *in silico* per valutare le variazioni di densità minerale ossea nel femore a distanza di un anno e sei anni dall'intervento. Le variazioni sono state inoltre esaminate separatamente nelle sette zone di Gruen (GZ). Infine, è stato elaborato un protocollo per indagare dove si verifica formazione e riassorbimento di tessuto osseo. Questo metodo è stato poi utilizzato per elaborare i dati di dieci pazienti per verificarne sia fattibilità che ripetibilità.
In questo studio di coorte sono state identificate alcune tendenze generali, ovvero un aumento percentuale di osso spongioso (in particolare in GZ 3 e 5) e una diminuzione per quello corticale (in particolare in GZ 1, 2, 6 e 7) sei anni dopo l'operazione. La perdita di densità ossea è localizzata in GZ 2, 3 e 6 per il gruppo cementato ed in GZ 1 per il gruppo non cementato. Inoltre, i risultati sulle formazioni ossee mostrano che si è verificato un riassorbimento osseo nella zona prossimale del femore un anno dopo l'intervento.
Con un ulteriore ampliamento di dati, questa metodologia fornirà uno strumento per trarre conclusioni sui fenomeni analizzati. Tale analisi sarà fornita ai chirurghi al fine di sviluppare nuove strategie non solo per quanto riguarda la selezione dell'impianto più congeniale, ma anche per quanto concerne il miglior approccio alla riabilitazione ed annessa terapia farmacologica.

Contents

List of Abbreviations

BMD Bone Mineral Density

BRUs Bone Remodeling Units

CT Computed Tomography

DEXA Dual-Energy X-ray Absorptiometry

GV Grayvalue

HU Hounsfield Unit

HXLPE Cross-linked Polyethylene

MDT Metal Deletion Technique

NJR National Joint Registry

OECD Organisation for Economic Co-operation and Development

PMMA Poly-methyl-methacrylate

PVE Partial Volume Effect

RIAP Registro Italiano ArtroProtesi

ROI Region Of Interest

THA Total Hip Arthroplasty

THR Total Hip Replacement

UHMWPE Ultra High Molecular Weight Polyethylene

List of Figures

List of Tables

Chapter 1

Introduction

1.1 The Hip Joint

The hip joint is a ball-and-socket synovial joint at the juncture of the femur and the pelvis. The rounded head of the femur forms the ball, which fits into the acetabulum (a cup-shaped socket in the pelvis) [1].

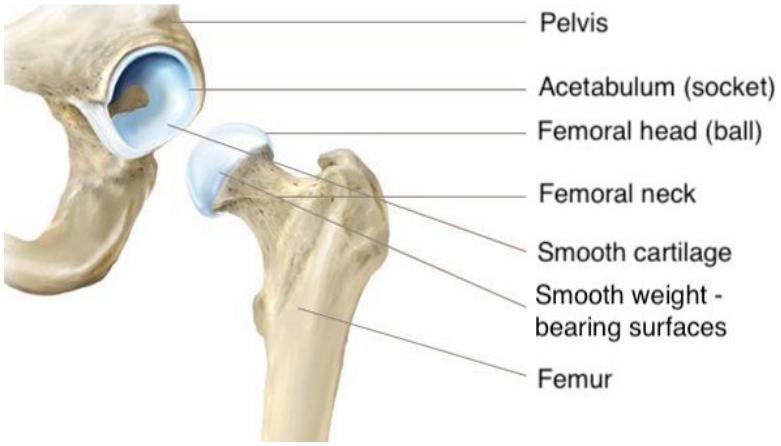

Figure 1.1: The articulating surfaces of the hip joint.

Both the acetabulum and the head of the femur are covered with articular cartilage, which is thicker at the places of weight-bearing. This connective tissue acts as a shock absorber, cushioning areas where bone meets bone and preventing abrasion and damage [2].

The primary function of the hip joint is to provide dynamic support to the body

while facilitating force and load transmission from the axial skeleton to the lower extremities, allowing mobility [3]. Indeed, the movements that can be carried out at the hip joint are flexion/extension, abduction/adduction and medial/lateral rotation (figure 1.2). The degree to which flexion at the hip can occur depends on whether the knee is flexed: this relaxes the hamstring muscles and increases the range of flexion. Instead, the extension at the hip joint is limited by the joint capsule and the iliofemoral ligament. These structures become taut during extension in order to limit further movement [4].

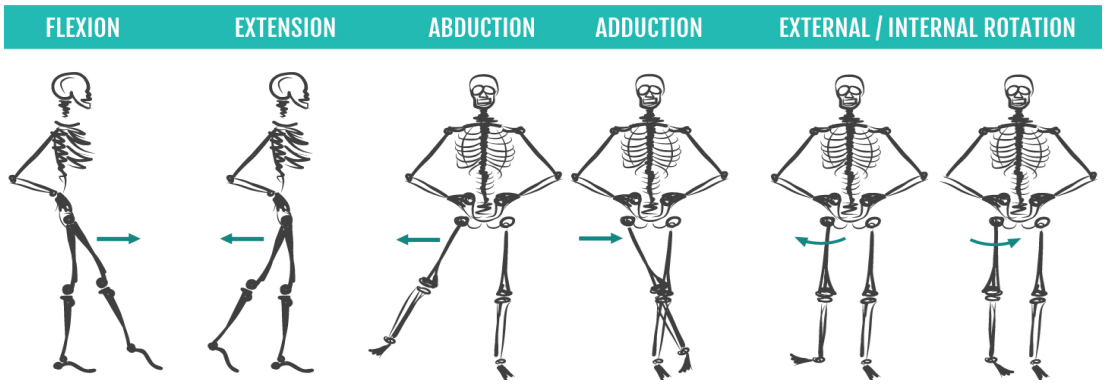

Figure 1.2: The directions of movements of the hip joint.

Several conditions can cause hip joint wear or damage, leading to a reduction in mobility and development of pain. The most recurrent pathology is osteoarthritis, which occurs when the protective cartilage that cushions the ends of bones wears down over time. Osteoarthritis is one of the ten most disabling diseases in developed countries. Worldwide, estimates show that 10% of men and 18% of women aged over 60 years have symptomatic osteoarthritis, including moderate and severe forms [5].

Certain other conditions that are highly likely to occur are osteonecrosis (that can result from a dislocation or fracture) and rheumatoid arthritis, an immunodeficiency disorder in which the immune system mistakenly attacks the lining of joints, causing bone erosion and joint deformity [6]. All these complications may lead to the need for a specific surgical intervention called Total Hip Arthroplasty (THA) or Total Hip Replacement (THR) [7].

1.2 Total Hip Arthroplasty (THA)

THA is a successful orthopedic procedure for the treatment of many crippling diseases that cause advanced hip joint damage. Two methodologies are used to fix the implant to the joint: one includes the use of cement, while the other is obtained by using the interference between the stem and the femur.
Since the early 1960s, improvements in joint replacement surgical techniques and technology have greatly increased the effectiveness of THA. Therefore, this surgical treatment has been widely used since its earliest recorded attempts. According to the Agency for Healthcare Research and Quality, more than 450,000 total hip replacements are performed each year in the United States [8]. Since 2007, the number of hip replacements has increased rapidly also in most OECD countries (figure 1.3). On average, hip replacement rates increased by 30% between 2007 and 2017 [9]. In Italy, the numbers of hip replacement surgeries have gone from 72,575 in 2001 to 102,378 in 2015 and these numbers are expected to increase over the years [10].

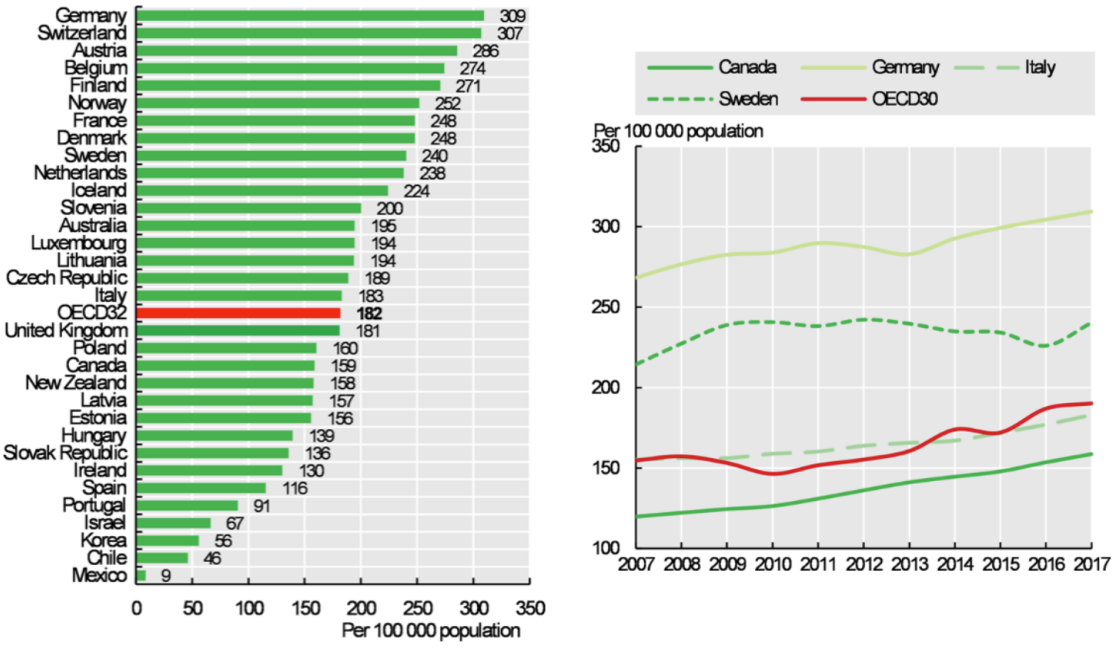

Figure 1.3: Statistics on THR. On the left, hip replacement surgeries performed in every country (2017). Iceland counts 224 operations per 100,000 people, Italy 183; on the right, hip replacement surgery trends in selected OECD countries, 2007-17 [9].

According to data collected by the Italian registry RIAP, women are most likely to undergo THA (60% of patients). The average age is 69.2 for men - with a standard deviation of 13.3 - and the largest age group for primary THA is 65-74 years old. For women, the average age is 74.7 (with a standard deviation of 11.6), while the largest age group is 75-84 years old [10].
The success rate for THR is high, with more than 95% of patients experiencing relief from hip pain. The success rate of hip replacements 10 years after surgery is 90-95% and at 20 years 80-85% [11].

1.3 The Hip Prosthesis

1.3.1 Components and materials

Historically, a replacement of the articulation of a human hip is simulated with the use of two components:

1. a femoral component (consisting of a *stem/pin* and *head*);
2. an acetabular cup (consisting of a *liner* and a *shell*).

The latter is fixed in the pelvis, while the femoral head is anchored in the femur by the stem. The acetabular cup consists of a shell in which a liner is inserted in order to provide the load-bearing articulating surface. Figure 1.4 shows the typical form and position of a hip joint prosthesis.

A great advantage relies on the modularity of the implant. Thus, it allows for the creation of *ad hoc* solutions, using different materials with properties most suitable for their function [13, 12]. Hip prosthesis components can be fabricated from different types of metals, ceramics, polymers and composites. Generally, polymeric materials alone are too weak, therefore, not suitable to meet the requirement of stress deformation responses in THA components. Metals have good mechanical properties but poor biocompatibility; besides, stress shielding effect and the release of dangerous metal ions can cause possible failures and may lead to the removal of implants. Ceramics usually have good biocompatibility but tend to be brittle.

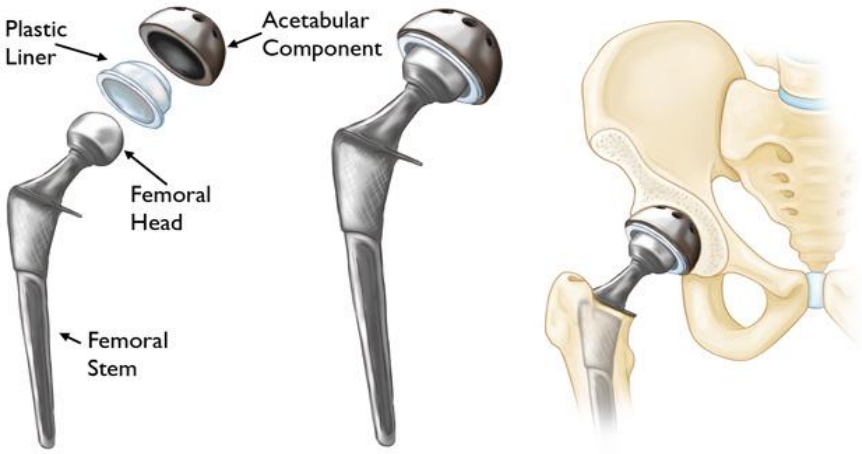

Figure 1.4: A hip prosthesis. On the left, its component; in the center, the components merged to form the implant; on the right, the prosthesis fixed into the hip. [16]

Figure 1.5: The three most commonly used bearing surfaces.

Several current studies are focusing on composite materials with engineered interfaces. This kind of materials may achieve the required mechanical strength, biocompatibility and toughness whilst being more malleable than metals. These characteristics reduce the stress-shielding effect [14, 15].
Hip prostheses can therefore be categorized based on the materials used for the combination between the femoral head and the acetabular cup. The most common combinations are metal-on-polyethylene (MoP) metal-on-metal (MoM) and ceramic-on-ceramic (CoC) (figure 1.5).

The femoral stem is subjected to the highest mechanical stress; hence, it must provide high number of load cycles (million per year) from the upper part of the implant to the lower limb. For this reason, only metals have been used for its

fabrication since metals have high mechanical strength and fatigue resistance as required [17]. Certain parameters, such as stem length and stem cross-sectional shape, should be taken into account in the design of the implant, given that they affect the load distribution [18].

The femoral head is connected to the neck by a Morse taper. The diameter of the femoral head plays a significant role in determining the feasible range of motion of the artificial hip joint and its stability against dislocation. Initially, 22 mm diameter metal heads were used. Throughout the years, the development of new materials and production techniques has led to the use of larger diameters (32, 36 and 40 mm) in order to counteract the problem of dislocation caused by the smaller femoral heads [19].
Femoral heads are usually made with metals or ceramic material, Co-Cr-Mo-cast alloys, stainless steel and alumina. The material and design must guarantee mechanical resistance to the tensile stresses that rise along the taper junction. Ceramic femoral heads feature a higher surface smoothness than metal femoral heads, resulting in a lower friction rate achievable. However, there are limitations in manufacturing larger diameters for ceramic heads, along with higher brittleness [20].

In contrast to the femoral head, the liner (also known as the socket) is mechanically locked into the shell. In hard-soft material coupling, the liner is made from polymeric materials, usually UHMWPE or highly cross-linked polyethylene (HXLPE). In hard-on-hard contacts, Co-Cr-Mo-cast alloys and alumina (pure or BIOLOX delta) or zirconia are used [21]. The liner is locked into the outer shell, which ensures mechanical stability of the acetabular cup, and the shell is then fixed into the pelvis via bone cement or press-fitting. In certain circumstances, screws are used to enhance fixation. The shell is always made with metallic materials, usually pure titanium or stainless steel, while the external contact surface is produced with a porous surface, with sintered titanium beads or hydroxyapatite, to stimulate bone integration [20].

In table 1.1, the most commonly used materials to fabricate every single component of THA prostheses are summarized.

Component	Material class	Most used material(s)
Femoral stem	Metal	Co-Cr-Mo wrought, Ti alloys
Femoral head	Metal	Co-Cr-Mo cast
	Ceramic	Alumina (pure or zirconia-toughened), zirconia
Acetabular cup liner	Polymer	UHMWPE, XLPE (cross-linked UHMWPE)
	Metal	Co-Cr-Mo cast
	Ceramic	Alumina (pure or zirconia-toughened), zirconia
Acetabular cup shell	Metal	Commercially pure Ti

Table 1.1: Materials used in THR prosthesis [20].

1.3.2 Fixation methods

As already mentioned in section 1.2, fixation of both the femoral stem and the acetabular cup can be achieved using acrylic bone cement (cemented fixation) or press-fitting against the bone (uncemented or cementless fixation). In a different methodology, known as hybrid fixation, the stem is inserted with the cement approach and the cup with the uncemented one. Another fixation option is referred to as reverse hybrid fixation, with a cemented cup and a cementless stem. However, this last method is rarely performed, representing only 1.7% of all THAs recorded by the Italian registry RIAP and 2.5% of total hip replacement performed in England, Wales, Northern Ireland and the Isle of Man according to the National Joint Registry (NJR) [10, 22]. An example of each one of these methods is shown in figure 1.6.

The rates of the different fixation options vary significantly from country to country. From 2010 to 2017, the use of the uncemented approach has increased in Norway (25%-38%), Denmark (68%-71%), and Sweden (15%-24%). In contrast, cementless fixation has slowly decreased during the past 7 years in England-Wales (43%-37.8%), Australia (65%-63%) and New Zealand (51%-48%), and it has almost halved in Finland (71%-49%). Switzerland had the highest number of uncemented fixation procedures, which is stable around 86% [23].

Both fixation methods are effective for pain-relieving and greater mobility, but they affect the patients in different ways.

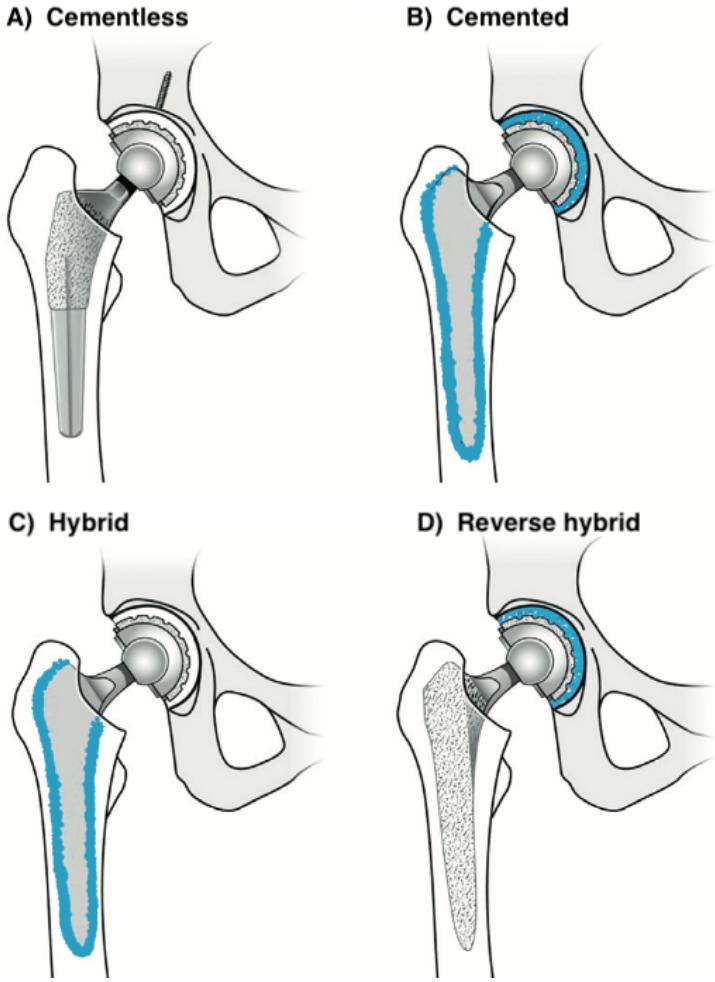

Figure 1.6: Overview of four different fixation options for the femoral stem and acetabular cup in THA. (A) Fully uncemented design. (B) Fully cemented design. (C) Hybrid design with a cemented stem and cementless cup. (D) Reverse hybrid design with a cemented cup and cementless design. For clarity, cement is shown shaded in blue [24].

The Cemented Method

The cement technique for use in THA was introduced by Sir John Charnley in the 1960s [25]. In cemented prostheses, the acrylic cement assures fixation of the implant to the bone tissue, whilst also facilitating uniform load distribution and

transfer across the whole contact surface between bone and implant [26]. Tipically, the material used for the cement is Poly-methyl-methacrylate (PMMA). PMMA does not bond the prosthesis to the bone, but works as a filler in the free space between bone and implant, acting as an interpositional layer to accommodate stresses caused by the difference in stiffness between the metal and the bone. Thereby, a homogeneous stratum of cement avoids the establishment of stress areas that would induce implant loosening or fractures [21].
The surgical technique is described below. Once the hip has been dislocated and the femoral neck resected, a reamer is used to create a hole in the femoral canal and then rasped to compress and remove the bone away. In the beginning, smaller rasp sizes are used until the templated size of the stem is reached. The final size of the rasp is 1.5–2 mm bigger than the stem in order to give space for bone cement [27]. Later, a plug is inserted into the femoral canal to prevent the cement from flowing to the distal part of the femur. Bone cement is then injected into the hollow femoral canal with compressor, followed by the stem. It is very important that the surgeon is rather quick in adjusting the stem placement due to the short handling time of bone cement [28].
After placing the stem component, reamer is used to remove the articular cartilage in the acetabulum in order to place the acetabular cup, which is fixed in the proper manner with bone cement.

The Uncemented (or Press-Fit) Method

Cementless THA uses mechanical press-fit contacts between the implant and the bone. Close surface contact is required in this application, as this facilitates bone integration. Moreover, the implant must have a porous coating or porous surface finish in order to promote bone on- and in-growth. On-growth surfaces are created by plasma spraying hydroxyapatite onto the component to create a textured surface, with multiple indentations onto which bone can grow. Meanwhile, in-growth surfaces are created using sintered beads, fiber mesh and porous metals. Such structures create microscopic pores (50–400 μm) into which bone can grow [29, 30].
Since it is not possible to take advantage of the PMMA cushioning effect, the

materials and design of the prostheses must also replace cement function. Indeed, uncemented stems are often made from titanium alloys, whose elastic modulus is significantly lower than Co-Cr-Mo alloys' ones. In addition, a more efficient fixation of both femoral and acetabular components is achieved by edgy and groovy designs, other than by using screws [20, 31, 32].

The surgical procedure starts with the hip dislocation and the osteotomy of the femoral neck. A reamer is used to locate the hole in the femoral canal and then rasped to make a bed for the stem. Rasps with increased size are used until good stabilization for the stem is reached. Each rasp size belongs to a specific size of stem, and are relatively smaller in comparison in order to produce interference [33]. The insertion is then carried out by using hammering blows that need to be carefully controlled in terms of force by the surgeon. This is because an excessive force, enhanced also by the wedge effect of the stem's shape, may result in a fracture.

Cemented vs Uncemented Implants

Several studies have been carried out to assess survival rates and clinical outcomes for both implant solutions [34, 35, 36]. The results of modern cemented and uncemented total hip arthroplasties are outstanding; however, each system has its advantages and disadvantages.

Cemented femoral component provides an immediate post-operative advantage in terms of better integration between bone, cement and the prosthesis, which permits a significant early relief of pain and early weight-bearing [37]. For this reason, cemented implants show higher survival rates in the short and mid-term [35]. However, the use of cement introduces some disadvantages. The degradation of PMMA can be a direct cause of loosening and in other cases is a secondary cause via particle-induced osteolysis [38]. These factors may often lead to a revision surgery, which is more complicated to perform in case of cemented implants rather than uncemented ones.

Although uncemented implants are more likely to go under revision in the first two years after surgery due to periprosthetic fractures, higher survival rates were observed in long-term period [39]. However, a bone quality assessment has to be

performed before choosing the press-fit method, since a low bone mineral density can result in an intra-operative fracture. Therefore, the uncemented approach is preferred for younger and more active patients, whereas for older people the cemented option is more likely to be chosen. Other factors, such as muscle quality and co-morbidities are considered while choosing the right implant [40]. Additionally, the female gender is often taken into account in orthopaedics final decision, where the bone density is often less in females compared to males [41].

1.3.3 Possible complications and failures

Despite successful outcomes, THA revision rates have grown steadily in recent years [42]. Increased life expectancy in a globally aging population is associated with the increased use of THA, resulting in increased revision rates. The three most common reasons for implants requiring revision are infection, technical errors at the time of surgery, and recurrent dislocation [43].
Identifying risk factors for THA failure is difficult because revision arthroplasty is relatively infrequent with late occurrence. Indeed, failure of a hip replacement requiring revision surgery occurs at a rate of approximately 1% per year for the first 15 years.
Risk factors for implant failure can be classified as patient factors, implant factors, and surgeon factors (figure 1.7).

Patient factors. Age, sex, and etiology of arthritis are the most important patient factors with a bearing on implant failure caused by aseptic loosening. A significant increase in failure rates in men compared with women is observed as early as two years after surgery. Furthermore, regardless of the underlying diagnosis, the younger the patient the higher the rate of implant failure [43, 44].
Deep infection occurs in around 0.5–2% of THR and is the cause for revision surgery in at least 7.5% of failures. Infection is more common in case of certain diseases, such as inflammatory arthritis and diabetes mellitus [45]. Dislocations can occur at a rate of almost 5%. Most of these will be single dislocations occurring in the early postoperative period, which are successfully treated by closed

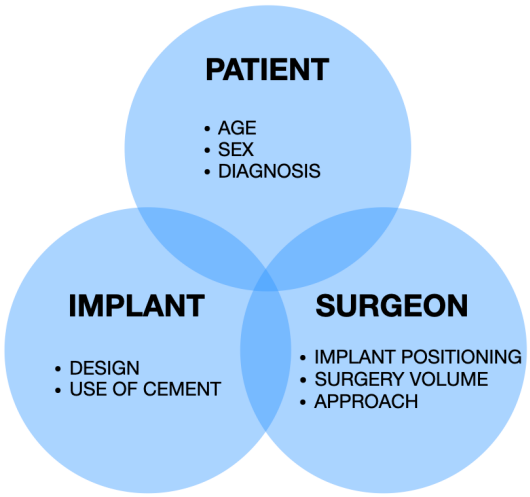

Figure 1.7: Factors related to total hip arthroplasty failure modes.

reduction. One in 30 revision arthroplasties is performed as a consequence of recurrent dislocation. Dislocation rates are increased in patients over 80 years of age. Indeed, poor muscular tone, femoral neck fractures and dystrophy are associated with an increase in dislocation rates [46].

Implant factors. As already mentioned before, the choice of the implant plays a key role in the long-term survival of the prosthesis. Uncemented implants were introduced in response to loosening seen in cemented systems. However, researches on countries where hip registries are maintained shows that the higher the percentage of cementless implants inserted, the higher the implant failure rate [43, 22].

Improvements in operative techniques and implant materials have led to decreased failure rates of hip replacements. Various changes in surface finish, stem geometry and cementing techniques are commonly adopted to achieve better outcomes. However, even small modifications have been found to have a significant impact on the final result, in some cases with detrimental effects [47, 48]. Moreover, many new implants are often used in absence of clinical review and fail to match the survival rates of earlier designs.

Surgeon factors. Surgical approach, preparation of the implant bed, and cementing techniques all reflect on implant survival. Dislocation rates do not seem to differ with surgical approach, but are higher when the surgery is performed by inexperienced surgeons [49]. Surgeons need to be trained properly to perform THR, but unfortunately training is difficult as the operation is complex and there is little evidence as to which are the best techniques to use. Although hip arthoplasty is a commonly performed procedure, it is not an easy operation to perform well and the implications to the patient are enormous if it is performed badly.

Nonetheless, many countries are adopting a registry for post-marketing surveillance in order to collect data on joint prosthetic performance. Through the registers, it is possible to evaluate the effectiveness of several of these risk factors – such as implant lifetime or surgical approaches [50]. Thereby, the healthcare resource can be used as an effective tool to select the best type of prosthesis and surgical technique for the treatment of specific cases.

1.4 Bone Remodelling after THA

Bone remodelling is a fundamental process through which the skeleton tissue is continuously renewed to maintain the structural, biochemical and biomechanical integrity of bone and to support its role in mineral homeostasis. Bone remodelling takes place on bone surfaces and is achieved through the cellular activity of a group of bone cells defined as bone remodelling units (BRUs) [51].
To assess bone remodelling before and after THA, periprosthetic bone mineral density (BMD) of the femur is determined. BMD quantifies the amount of bone minerals per cubic centimeter, providing a measure of bone gain and loss on the same region through the years. Bone density measurement is used in clinical medicine as an indirect indicator of osteopenia/osteoporosis and fracture risk [52]. Several methods are used to evaluate BMD. These tests include:

- Dual-energy X-ray absorptiometry (DEXA);
- Computed tomography (CT);

- Quantitative ultrasound (QUS);
- Digital X-ray radiogrammetry (DXR);
- Dual photon absorptiometry (DPA).

The first two are the most widely used technique for BMD assessment in clinical and research practice. Therefore, these methods will be further described.

The DEXA test works by sending two low-dose X-rays which are absorbed differently by bones and soft tissues (figure 1.8,a). The density profiles from these X-rays are used to calculate bone mineral density. Results are then scored by two measures, the T-score and the Z-score. The former represents the bone mineral density at the site when compared to a healthy 30-years-old adult, while the latter compares the BMD to the average bone density of people of the same age and gender. Patients with a T-score of -1.0 or higher have a normal BMD, a score between -1 and -2.5 indicates a low bone mass (osteopenia), whereas a value under -2.5 is a sign of osteoporosis.
The main advantages of DEXA are its wide availability and short scanning times; however, subjects are exposed to a ionized radiation which depends on the machine. Nonethless, the radiation dose is minimal compared with that given by many other investigations involving ionizing radiation [53]. Another important shortcoming of DEXA is that it measures bone in two dimensions providing only an estimation of bone density.
The use of Hounsfield units (HU) from CT scanning to assess BMD has recently been described, with several subsequent studies exploring its utility in assessing fracture risk [54]. Hounsfield unit values are a measurement of the standardized linear attenuation coefficient of tissue, based on a defined scale where water is arbitrarily defined to be 0 HU and air is defined as -1000 HU. Modern radiology imaging software programs allow this to be calculated from a region of interest (ROI) on CT scans without any additional cost or radiation exposure. Values are calculated based on the following formula:

$$HU = \frac{\mu_X - \mu_{water}}{\mu_{water}} \cdot 1000 \tag{1.1}$$

where μ_X is defined as the linear x-ray attenuation coefficient of the selected voxel and μ_{water} the attenuation coefficient of distilled water at room temperature and pressure. By calibrating the CT scanner with a phantom, it is possible to define the relationship between HU and BMD. A typical configuration of this imaging device is shown in figure 1.8,b.

Computed tomography (CT) has some important advantages compared with DEXA since it provides a three-dimensional assessment of the examined bone, in addition to a separation of cortical and trabecular bone [55]. However, a single voxel may contain various type of tissue because of the finite spatial resolution of the CT scan. This artifact is related to a phenomenon called partial volume effect (PVE), which occurs when tissues of widely different absorption are encompassed on the same CT voxel producing a beam attenuation proportional to the average value of these tissues. Furthermore, the metal from hip implant produces streak artifact on CT scan, thereby adversely affecting image quality. PVE and metal artifacts complicate the segmentation process, thus several techniques are adopted to reduce them.

Another significant disadvantage of the CT scanning technique is its high-radiation dose (1.5 mSv[1]).

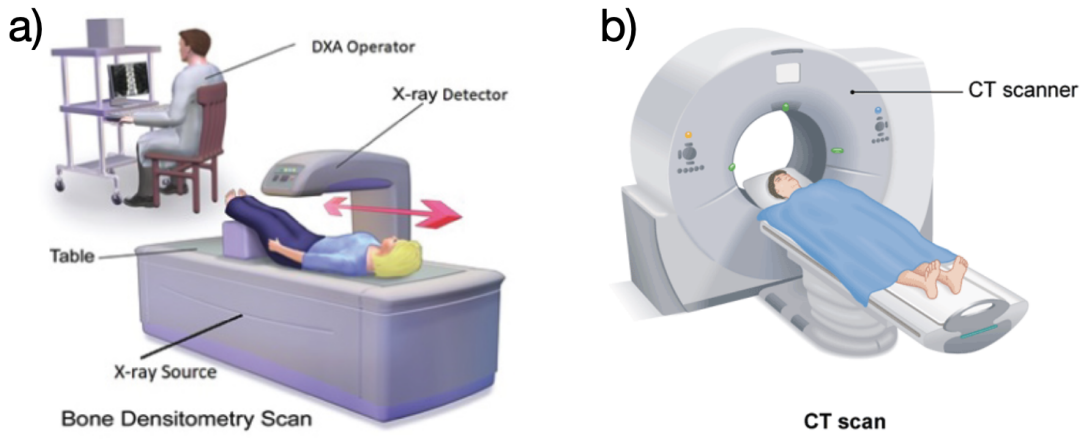

Figure 1.8: Medical imaging techniques used to assess bone mineral density. a) A typical DEXA system configuration; b) a modern CT scanner.

[1]The sievert (Sv) is a derived unit of ionizing radiation dose in the International System of Units and is a measure of the health effect of low levels of ionizing radiation on the human body.

1.4.1 Factors influencing bone remodelling

Bone remodelling varies within and among the different bones of the skeleton and this variation changes with age, underlying the mechanism of age-related bone loss [56]. Indeed, the aging process causes loss of bone mass, resulting in the demineralization of bone matrix. This issue is more commonly seen in women, since the hormone changes that happen at the menopause directly affect bone density [57]. Another age-related effect is the reduction in toughness of bones, which become more brittle and more susceptible to fracture [58].

In addition to aging and sex, several factors can affect bone remodelling after THA. After the insertion of the stem, mechanical loading forces in the entire periprosthetic femur are redistributed. As a consequence, the bone remodels to adapt to the new environment by changing its bone mass.
Various studies regarding this topic have been conducted over the years, with a follow-up period ranging from 18 months to 5 years post-operation [59, 60, 61, 62, 63]. In all these studies, the bone mineral density was calculated with DEXA in seven regions of interest surrounding the femoral component, according to the standard Gruen analysis protocol shown in figure 1.9 [64]. Results show that the most significant bone loss occurs in ROI 7 and it is most likely to be observed in ROI 6 if a cemented implant has been used [59, 62, 63]. Indeed, an increase in BMD, even if minimal, is detected particularly using uncemented prosthesis. This proves that factors – such as the extent of the porous coating used in cementless stem – are relevant [65]. Bone mineral density changes in the distal areas (zone 3, 4, 5) are highly dependent on the size and stiffness of the implant, along with the proper placement of the stem in the intra-medullary cavity [61, 63]. With regard of ROI 1, a gain in bone density is observed with stems that bow posteriorerly, as this geometry achieves maximal contact with the bone [66].

In summarising the factors that influence bone remodelling, these include size, geometry and stiffness of the implant, as well as the presence and the extent of a porous coating. However, the main determinant of bone mass redistribution is stress-shielding at the implant-bone interface [67]. If stresses are too high, bone

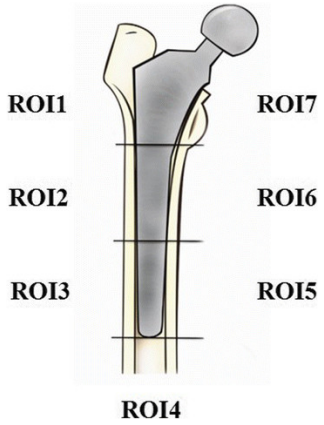

Figure 1.9: The location of the seven regions of interest (zone 1 to zone 7), defined according to the length of the inserted stem.

necrosis or periprosthetic fractures can occur. On the opposite side, bone atrophy is observed where bone is less loaded than normal, accordingly with Wolff's Law. In both cases a mobilisation of the implant takes place, resulting in a need for implant revision. A short outline of the mechanical behaviour at the implant-bone interface is shown in figure 1.10.

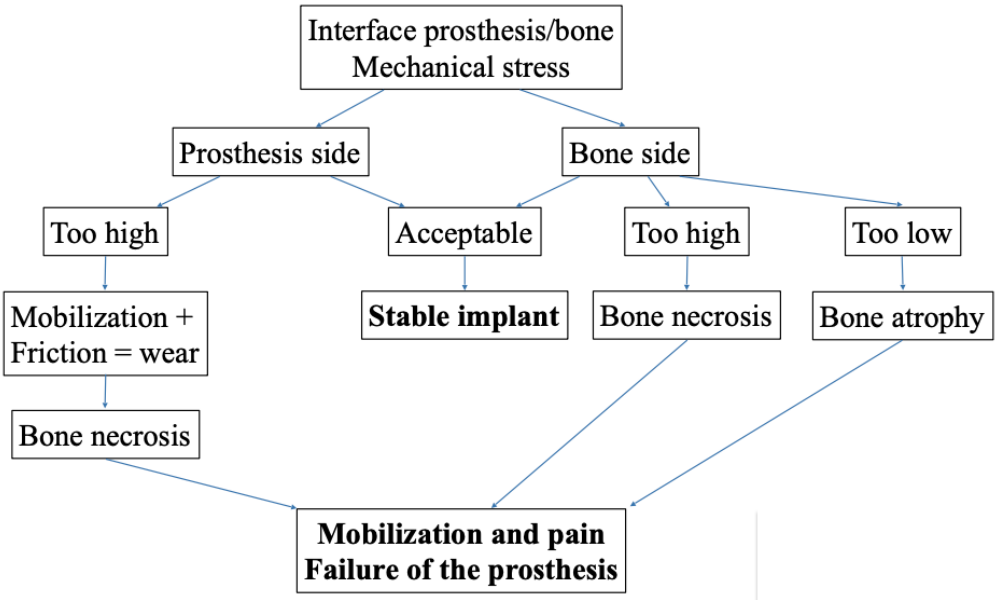

Figure 1.10: Mechanical behaviour at the prosthesis-bone interface [68].

1.5 Aim of the Thesis

According to the follow-up protocol developed by Landspitali – University Hospital of Iceland and University of Reykjavik, patients undergo CT-scans 24 hours, 1 year and 6-7 years after total hip arthroplasty. Based on BMD measurements by means of these three CT-scans, this study's aim was to develop a protocol to assess mineral density changes of the femoral bone in such time frame. Indeed, by checking any increase/decrease of density values around the prosthesis, an accurate estimation of bone remodeling is provided.

As suggested in previous works, CT-based densitometry measurements were processed through the image processing software Mimics[2], and thus employed for developing an *in silico* method to assess proximal femur's BMD evolution one year and six years post-operatively [69]. Any difference in mineral density was also evaluated separately in the seven standard Gruen zones. Furthermore, a protocol was developed to evaluate where bony formations/resorptions are to occur. Several new tools were assessed in order to reduce the inter- and intra-operator variability in certain steps. The protocol was then applied to process 10 patients' data (3 females with a cemented prosthesis, 2 females and 5 males with an uncemented prosthesis) to verify its feasibility and repeatability.

The novelties of this method are manifold. First of all, a volumetric quantification of bone gain and loss is made possible, as well as the visual localisation of its three-dimensional distribution. Furthermore, no other longitudinal study using the CT-scan technique has been carried out for such a long time.

[2]Materialise NV (Leuven, Belgium)

Chapter 2

Materials and Methods

2.1 Study Workflow

Figure 2.1 shows a scheme of the workflow for the evaluation of bone mineral density changes and new bone formations occurring in the femur one year and six years after THA. This study stems from the synergic collaboration with colleagues of the Department of Biomedical and Neural Engineering at Reykjavik University.

First of all, data from study participants were collected. For each patient, three CT-scans were provided following a structured scanning protocol: the first one was carried out 24 hours after surgery, the second one after 1 year and the last one 6-7 years post-operatively. CT images were then segmented and, subsequently, re-sliced.
To assess mineral density changes, a comparison between post 24h and post 1y CT-scans and thereafter between post 1y and 6-7y was conducted. Femurs were divided in the seven regions according to the standard Gruen analysis already mentioned in subsection 1.4.1, thus evaluating any specific BMD change in those specific areas over the years. Finally, new bone formations were assessed.

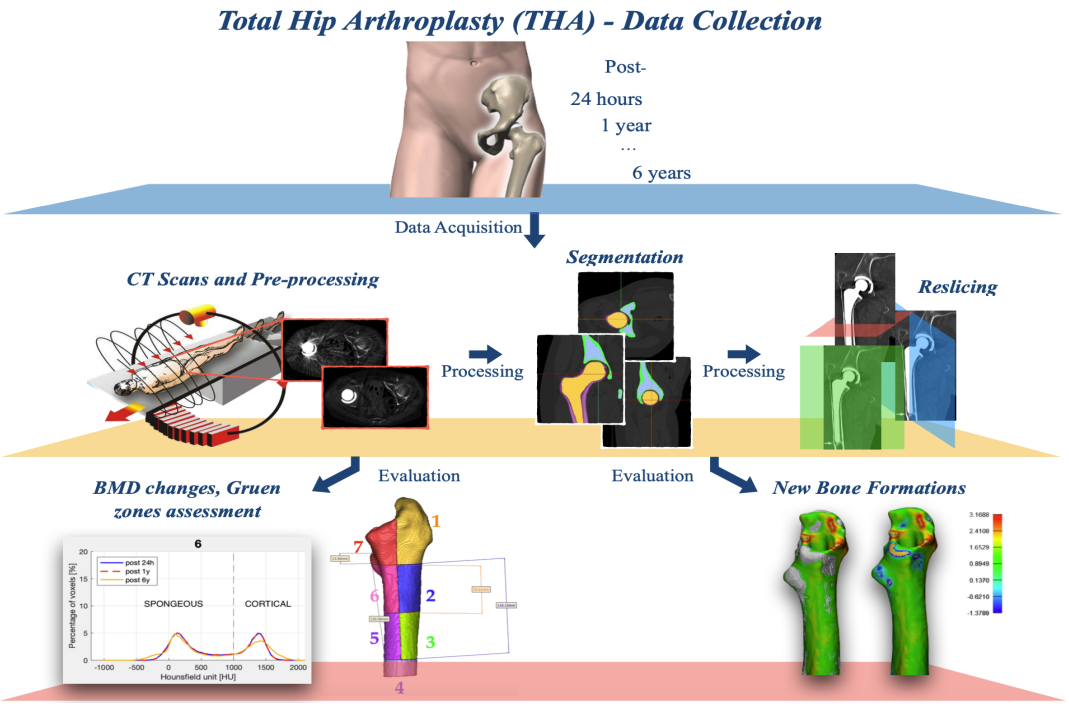

Figure 2.1: Study Workflow.

2.2 Study Cohort

The aforementioned methodology to evaluate BMD changes was carried out on patients that were already enlisted in the "Clinical evaluation score for Total Hip Arthroplasty planning and post-operative assessment" project. This research is the result from the collaboration between the University of Reykjavik and Landspitali – University Hospital of Iceland, therewith obtaining ethical approval from the local bioethics committee. The whole cohort of the project includes patients undergoing primary THA surgery, either in uncemented or cemented setting. Some participants underwent unilateral THR, while others had bilateral THR.
In this research project, a total of ten patients was selected from this cohort including only those with an unilateral arthroplasty, so that the operated femur could be compared with the un-operated one. Seven subjects (five males, two females) had a cementless implant, three subjects (all females) a cemented one. The youngest patient was 57 years old at the time of the operation, whereas the oldest was 75. Average age was 62.3 $\pm$ 8.9 years. Informations including patients' sex, age and type of implant are summarised in table 2.1.

Patient Nº	Sex	Type of implant	Age	Operated side	Year of operation
1	Female	Cemented	70	Left	2013
2	Female	Cemented	74	Left	2014
3	Female	Cemented	75	Left	2013
4	Female	Uncemented	57	Right	2014
5	Female	Uncemented	63	Right	2014
6	Male	Uncemented	50	Left	2014
7	Male	Uncemented	52	Right	2014
8	Male	Uncemented	56	Right	2014
9	Male	Uncemented	59	Left	2013
10	Male	Uncemented	67	Right	2013

Table 2.1: Information about study participants. "Age" refers to the age of subjects when primary THA was performed.

2.3 CT Acquisition

Spiral CT scans of the patients' femurs were taken, ranging from the anterior superior iliac spine to the distal part of the femur at 24 hours, 1 year and 6-7 years post-operatively. The first two scans were acquired with a *Philips Brilliance 64 Spiral-CT* machine, the latter with a *Toshiba Aquilion PRIME*. The main technical specifications of these two scanners are shown in table 2.2.

	Philips	Toshiba
X-Ray Tube Current	249 mA	600 mA
Kilovoltage Peak (KVP)	120 kVp	120 kVp
In-plane resolution	0.5 mm × 0.5 mm	0.3 mm × 0.45 mm
Slice thickness	1.0 mm	0.50 mm

Table 2.2: Technical specifications of the two CT-scanners used.

In both machines, image reconstruction matrixes consist in 512 × 512 pixels. This means that every slice has such quantity of pixels, each of them represented by a grayvalue (GV) belonging to a 12-bit representation scale (4096 different levels of gray, from -1024 to 3071). Each GV has a corresponding value in the HU scale, according to the relation:

$$[GV] = 1024 + [HU] \tag{2.1}$$

An example of a CT-scan image obtained with *Toshiba Aquilion PRIME* can be seen in figure 2.2.

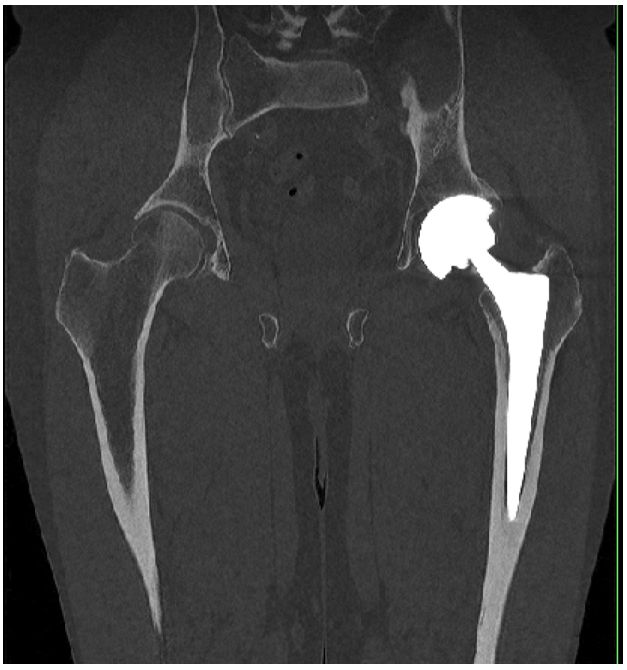

Figure 2.2: Coronal view of a CT-image.

2.4 CT Calibration

A calibration phantom (Micro-CT HA Phantom, GmbH, Möhrendorf, Germany) was used to find a mathematical relationship that could convert the CT-Scan values (in $[HU]$) into apparent density, i.e. BMD (in $[g/cm^3]$) (figure 2.3,a). This phantom includes five cylindrical inserts containing known densities of calcium

hydroxyapatite (CaHA), respectively to 0, 50, 200, 800 and 1000 HU. The physical densities for these five values were included in the datasheet and therefore shown in fig. 2.3,b with red dots [70].

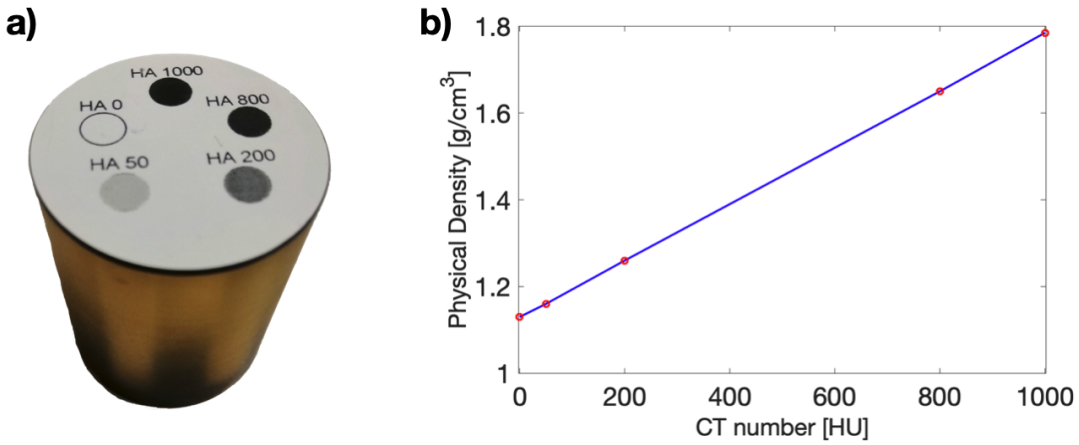

Figure 2.3: Micro-CT HA phantom. a) An image showing its configuration; b) The relationship between density and Hounsfield Unit in the phantom.

The same CT acquisition protocol was used as for the patients: slice increment of 0.3 mm, slice thickness of 0.5 mm and the tube intensity set to 120 KVp. CT-scans were then imported to Mimics for segmentation process. Hence, the masks from those five areas were created. Next, the Hounsfield values of each mask were exported as text files and imported to Matlab, where average HU value of each rod was calculated (table 2.3).

Hounsfield Units [mgHA/cm³]	Average HU values
0	55
50	119
200	335
800	1108
1000	1459

Table 2.3: Known HU values and their corresponding average HU values.

Afterwards, the "Curve Fitting" tool was used to find the interpolant between the calculated average values in tab. 2.3 and their physical densities in fig. 2.3,b. The resulting formula was:

$$\rho_{app} = 0.000494 \cdot HU + 1.1 \qquad [\frac{g}{cm^3}] \tag{2.2}$$

By using the equation 2.2, the conversion between Hounsfield Units and BMD has made possible (fig. 2.4).

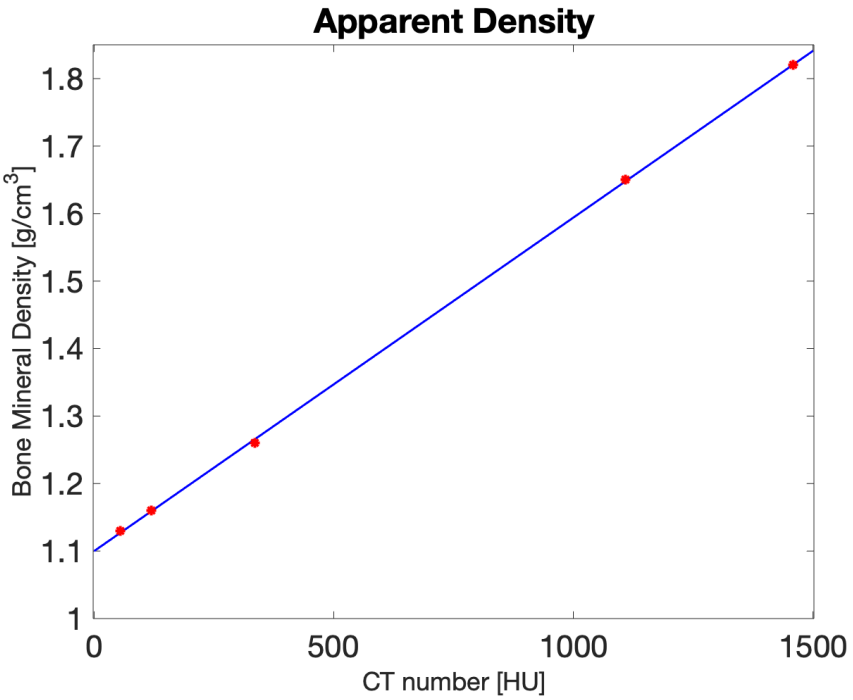

Figure 2.4: Plot from density calculations against their HU value.

.

2.5 Scatter Reduction

Data from CT-scans were corrupted due to several type of artifacts, including noise, beam hardening and metal artifacts. The latters introduced brigther streaks in images, thus modifying HU values around the prosthesis and therefore bone density.

To reduce such problem, CT images from the three datasets (post 24h, post 1y and post 6y) were imported into Mimics, where a scatter reduction was perfomed through "Reduce scatter" tool. This function is a new feature within Mimics, requiring the operator to create a mask with HU values higher than 3000. The mask obtained represented the metal implant, from whence the scatter was originated. Using this parameter and therefore setting the filtering strength to 100%, artifacts were reduced.
In previous protocols, an automatic software called Metal Deletion Technique (MDT) from ReVision Radiology had been used [71]. By means of this approach, artifacts were iteratively reduced slice by slice and then the image was then reconstructed. This method required several hours (from 6 to 13) to be finished, whereas the Mimics built-in function to reduce scatter required approximately 15 minutes to run out. In figure 2.5, an example of pre- and post-processed images with both techniques is shown.

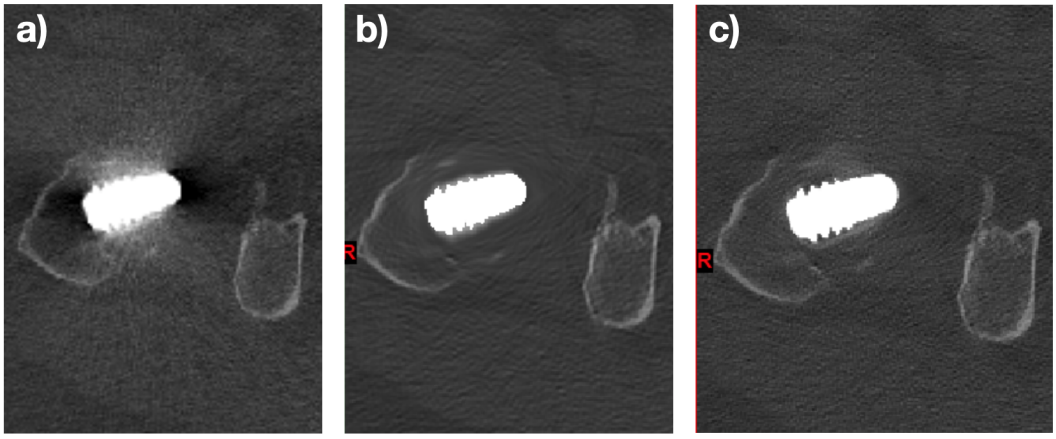

Figure 2.5: Pre- and post-processed CT-scans. a) A CT slice before artifact reduction; b) A slice processed wirh MDT technique; c) A slice after "Reduce scatter" tool.

2.6 Segmentation

A segmentation process was performed to isolate anatomical objects of interest for BMD analysis in the three datasets. Since both the operated femur and the controlateral femur were taken into account, a protocol was developed to differen-

tiate these areas. To reach this goal, a new mask was created with values ranging from 250 HU to 2999 HU. Indeed, by converting these numbers in apparent density through the calibration formula (eq. 2.2), acceptable values for bone mineral density are found, according to the literature and previous studies [72, 73, 74]. A function called "Split masks" was then used to partition the operated femur and the healthy femur from the rest of the bones. Using this tool, the operator was required to select the boundaries of the different areas of interest. A curve or a line was drawn for the first and the last slice where two different areas are put in contact, i.e. the un-operated femur with the hip bone. The same operation was carried out in an in-between slice. With an automatic interpolation, both areas of interest are then partitioned from the rest, as shown in figure 2.6.

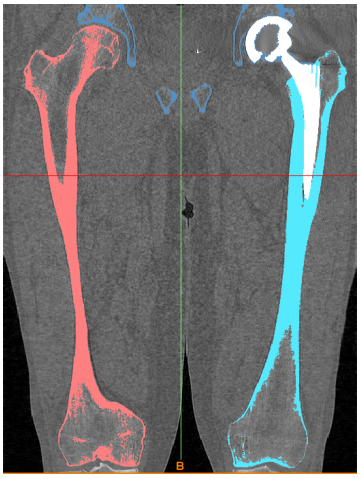

Figure 2.6: Masks for the operated femur (cyan) and for the un-operated femur (red), distinguished from the rest of the bones (blue). Masks were obtained using "split masks" tool.

The choice of 250 HU as the bottom level of the threshold rather than a lower value has two implications. Firstly, it simplifies the distinction between the different areas of interests. Secondly, it excludes small portions of the pixels identifiable as trabecular bone. As a result, a function called "Smart fill" was employed to fill the regions inside both femurs. A hole closing distance of 4-5 pixels was chosen, thereby images were scrolled and manual corrections were applied when needed. After performing such operations, a mask for the implant was created by taking each value above 3000 HU. A morphological operation of dilation was then carried

out, choosing one pixel as a parameter. Later, a boolean operation of subtraction was performed between the dilated implant and the operated femur to remove pixels from the stem, thus creating a cavity in the femur. In addition, both the unoperated and the operated masks were eroded by two pixels. These two operations were done to reproduce a small gap (approximately 1.5 mm) between the prosthetic implant and the bone, other than reducing some artifacts due to PVE. Afterwards, objects from the un-operated femur, the original implant and the operated femur were created from their respective masks. A wrapping (smallest details 0.75 mm, gap closing 0.5 mm) and a smoothing (3 iterations, smoothing factors 0.7 mm) were further performed. Finally, HU values for these 3 objects were exported as text files and imported to Matlab to assess BMD changes over time. An example of the 3 objects created is shown in figure 2.7.

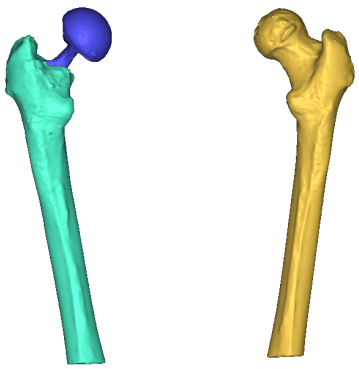

Figure 2.7: Objects created from masks for the operated femur, un-operated femur and the implant.

2.7 Reslicing

Subjects' body position inside the CT-scanner may vary even significantly not only from one patient to another, but also for the same subject in the three different datasets. Indeed, different degrees of abduction/adduction and internal/external rotation can be identified while looking at several CT-scans (figure 2.8). Therefore, a reslicing operation is required to realign the legs in the same direction, hence facilitating the comparison between patients' femurs over the years.

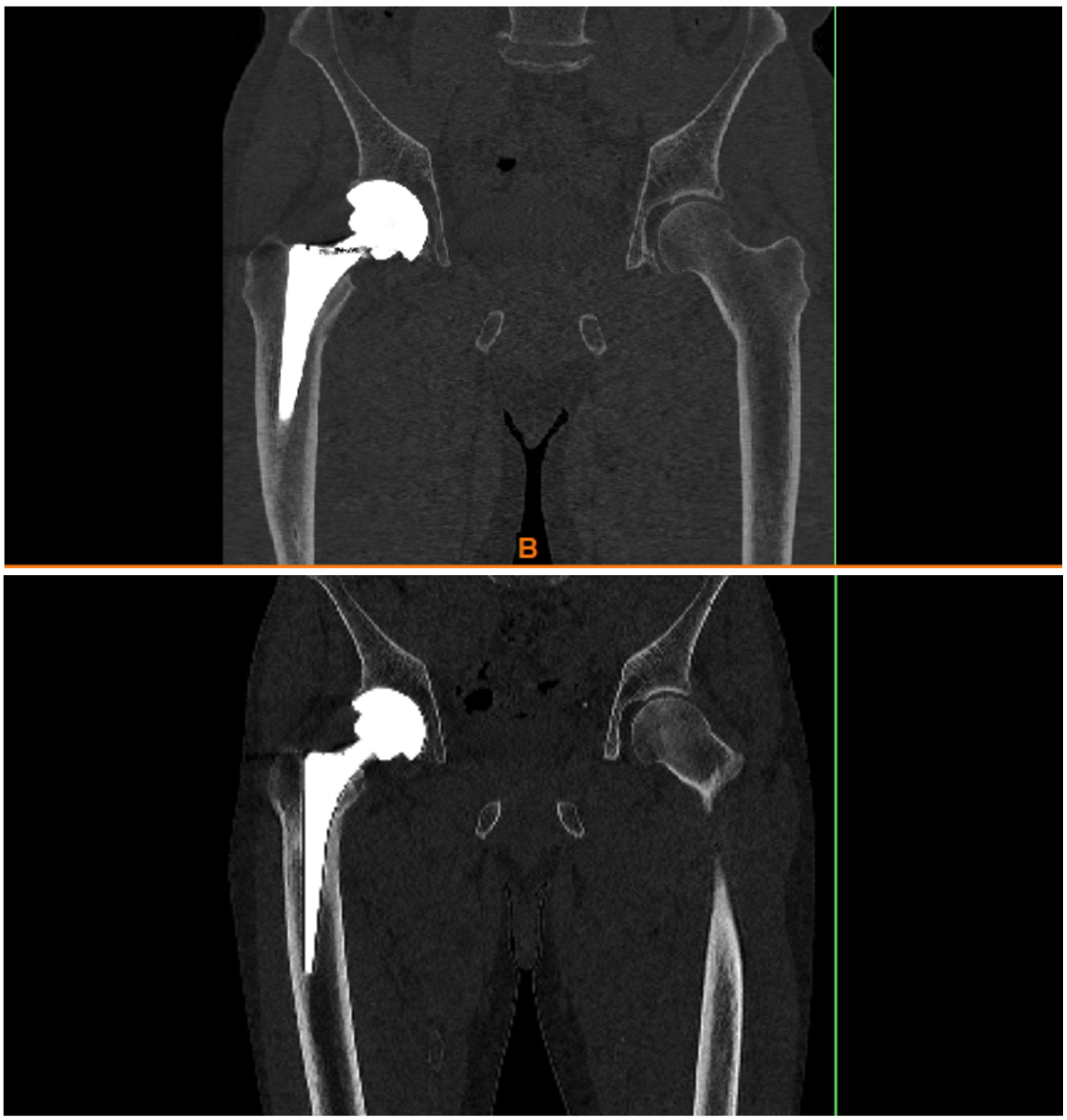

Figure 2.8: CT slices of a post 1y scan (above) and a post 6y scan (below) from the same subject. A different level of abduction can be observed between the two images.

To fulfill this task, the "Reslice images" tool in Mimics was used. Throughout this function, an alignment of body orientation was achieved by drawing a straight line passing through the longitudinal axis of the femur. Areas of interest were thus cropped, namely the operated femur and the un-operated femur. To allow an easier comparison between the three datasets, the line was traced starting from 2 cm below the distal part of the stem's tip and ending 5 cm above the proximal

extremity of the implant. All the masks previously created were automatically moved on the new resliced image.

Moreover, pixel size was uniformed, since this parameter could be different between post 24h, post 1y and post 6y CT-scans. The lowest value of the three datasets was chosen as standard and applied to the other two images, given that it provided the best result in terms of resolution. An example of a resliced CT-scan is shown in figure 2.9.

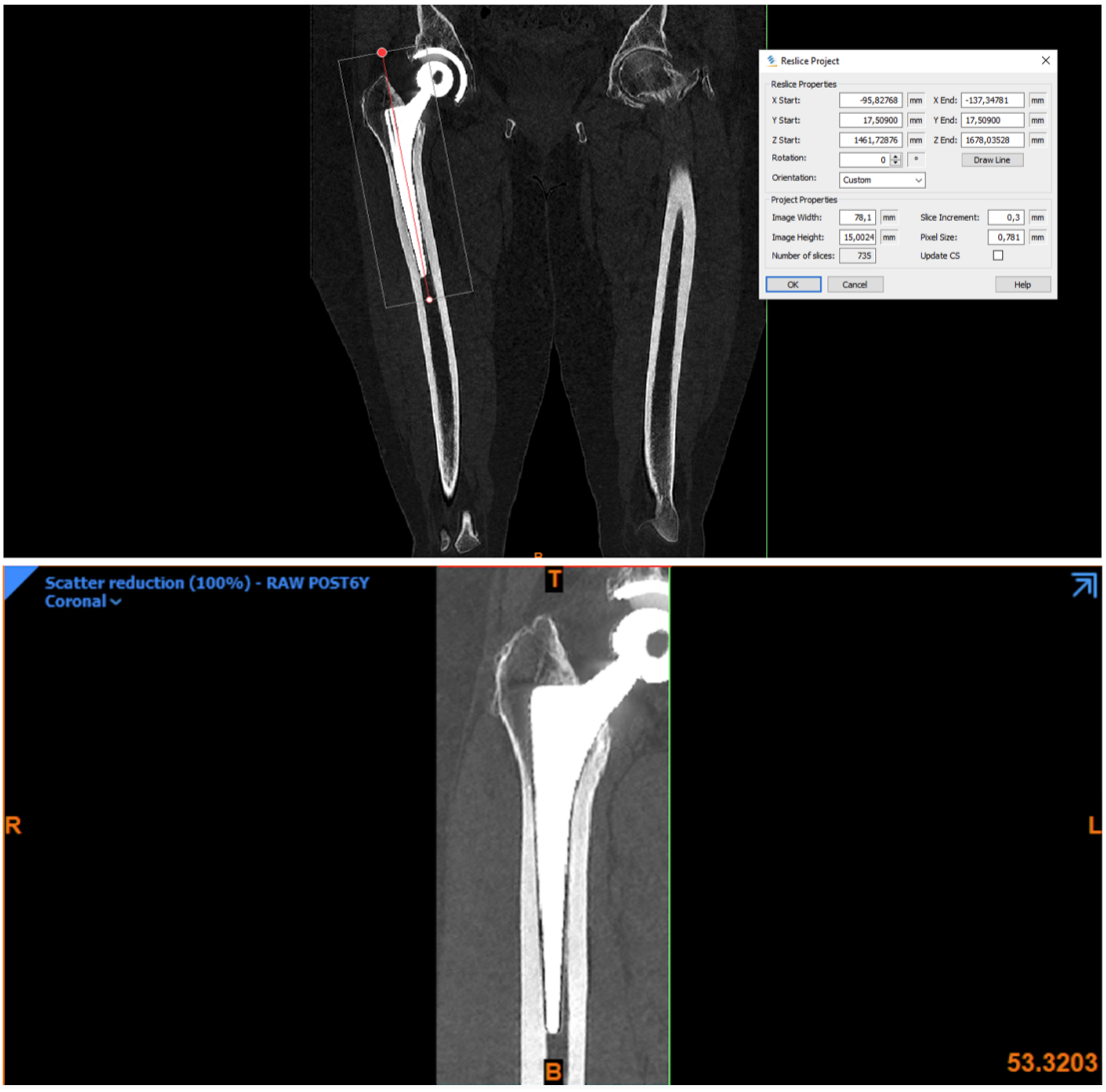

Figure 2.9: Mimics project before (above) and after (below) reslicing tool.

2.8 BMD Evaluation in Gruen Zones

A specific evaluation of bone remodeling throughout the years was investigated in the seven Gruen zones already defined in section 1.4.1. Such analysis was carried out to assess the occurence of patterns in bone remodeling, for instance depending on sex, type of implant etc.
The protocol of defining these regions was as follows:

- The 3D mask of the operated femur was set to the frontal view;
- A plane passing through the longitudinal axis of the femur was drawn by using "Cut orthogonal to screen" tool;
- The tip of the lesser trochanter was then identified and a plane passing through that point was drawn. Masks for Gruen zone 1 and 7 were then created;
- Another orthogonal plane going through the distal tip of the prosthesis was drawn;
- The distance between these last two planes was measured and a final plane was drawn at the midpoint. Masks for Gruen zones 2, 3, 5 and 6 were thus defined;
- The mask for Gruen zone 4 was created by merging the two regions under the implant.

All the masks thus obtained were then exported in .txt format and then processed on Matlab to assess the gain or loss in density for each Gruen zone individually.

The same approach was used to create the seven masks for the unoperated femur. Since no implant was present for the contra-lateral leg, the same distances measured for the operated leg were used. An example of the seven masks obtained for both femurs are shown in figure 2.10.

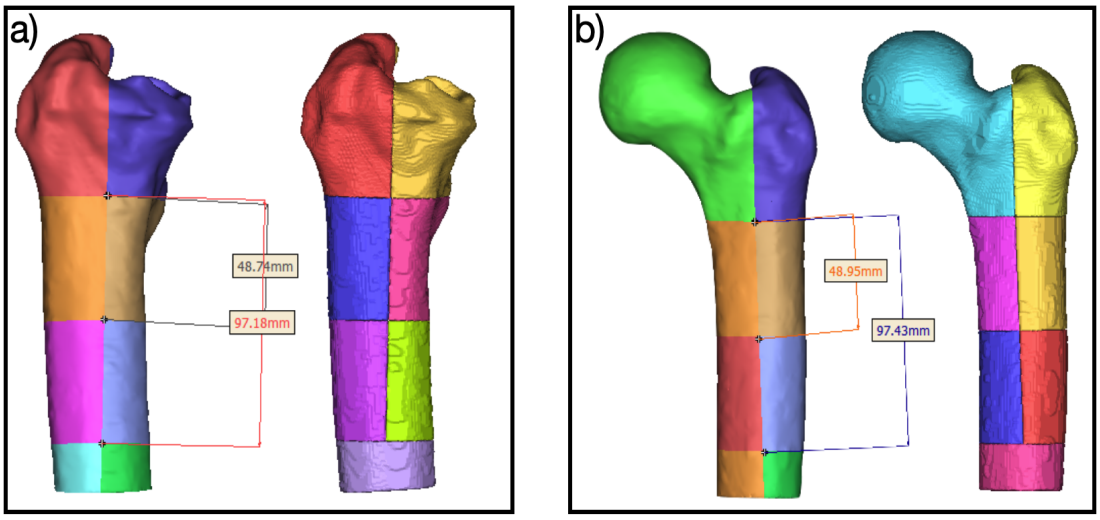

Figure 2.10: The bone after being cut in planes (on the left) and the seven masks created for the Gruen zones (on the right) for both the operated femur (a) and the unoperated femur (b).

2.9 New Bone Formations

To better localise where new bony formations occur, a point based analysis in 3-Matic software was used. This tool allows a comparison of the femur model at T2 (target entity) to the femur model at T1 (reference entity), measuring the distance (in millimeters) between each triangular node forming the 3D mesh from the target to the surfaces of the reference model. When comparing two masks, the most recent one was used as the reference (T1) and the oldest as the target (T2). For instance, using post 1y and post 24h masks, the former was chosen as T1 and the latter as T2.
A pre-alignment of the two objects was performed through "N points registration tool", thereby hand selecting these landmarks:

1. the middle tip of the lesser trochanter;
2. the protuberance under the greater trochanter;
3. the top of the greater trochanter.

Afterwards, a "Global registration" was applied to achieve the best alignment possible. The part comparison analysis was then carried out.

This analysis calculates the mean, minimum, and maximum values of the distances between the two entities, then produces a color map, as shown in figures 2.11 and 2.12. The operator is allowed to change the upper and lower thresholds of the distances such that all triangles are colored as follows:

- Blue (minimum part analysis): if the triangular node traveled a distance below the minimum threshold value (values are negative);
- Red (maximum part analysis): if the triangular node traveled a distance above the maximum threshold value (values are positive);
- Green: if the triangular node traveled a distance within the threshold boundaries.

Since just a semi-quantitative 3D localisation was required, thresholds were simply left to be the maximum and the minimum distances reached by every comparison. Indeed, the aim was just to assess if there were some specific regions where new bony formations were more likely to appear, or whether these phenomena were completely patient-specific. An example is shown in figures 2.11 and 2.12.

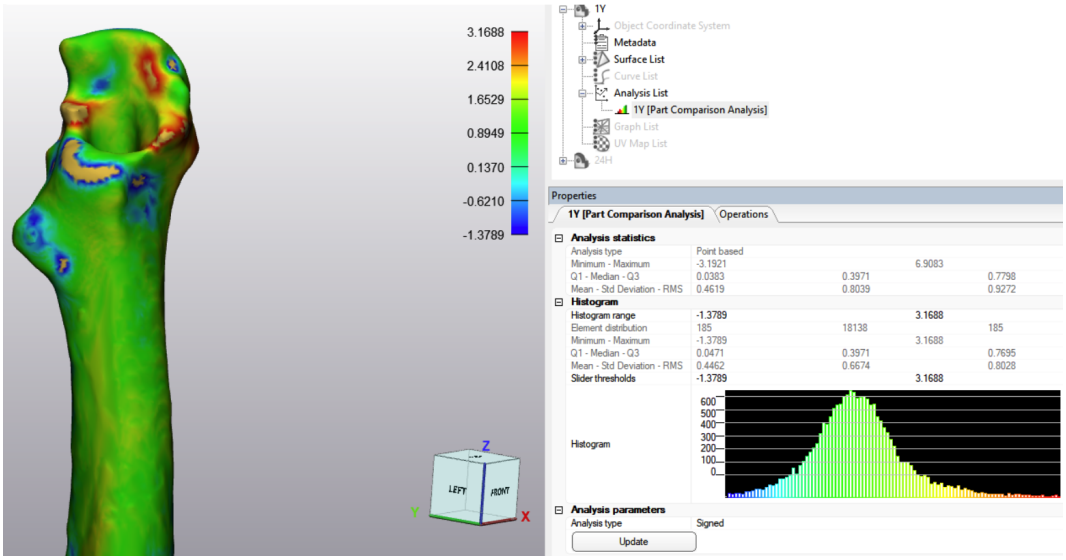

Figure 2.11: "Part comparison analysis" between post 24h and post 1y masks. On the left, the 3D localisation of bony formations/losses; on the right, the histogram showing the distribution of the number of elements and the relative distance between the two masks.

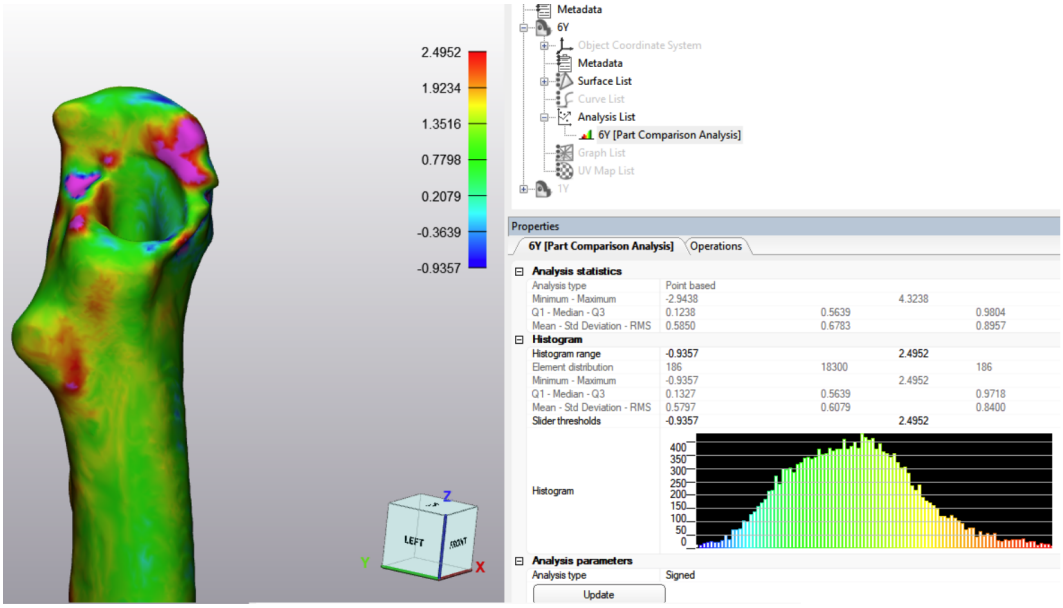

Figure 2.12: "Part comparison analysis" between post 1y and post 6y masks. On the left, the 3D localisation of bony formations/losses; on the right, the histogram showing the distribution of the number of elements and the relative distance between the two masks.

Chapter 3

Results

3.1 Bone Mineral Density Changes

Operated/Unoperated Femur

For each patient reported in table 2.1, bone mineral density changes in both operated and unoperated femurs were evaluated comparing the masks obtained 24 hours, 1 year, and 6 years post-operatively.

Figure 3.1 shows average values and the standard deviation for the whole cohort. To obtain the percentage rate, each number of voxels corresponding to a BMD value was normalised dividing by the total volume of the mask and multiplying by 100. Moreover, a black dotted line was used to differentiate the density values corresponding to spongeous bone from those corresponding to cortical bone. To this aim, a threshold was chosen at 1.4310 g/cm^3 (670 HU), since several studies suggest this value to be in the range that best identifies the cortico-cancellous interface [75, 76]. Blue, red, and yellow distributions represent the changes for operated (fig. 3.1,a) and unoperated femurs (fig. 3.1,b) at 24 hours, 1 year, and 6 years respectively.

The data showed a great variability among subjects, as proven by the relatively high standard deviation, reaching a range of $\pm$ 40% in the worst case scenario. Nevertheless, it is clear that a lower amount of spongeous bone occurred in the operated side rather than the unoperated side, since the average percentage of voxels in correspondence of the spongeous bone peak differs by more than 2.5%.

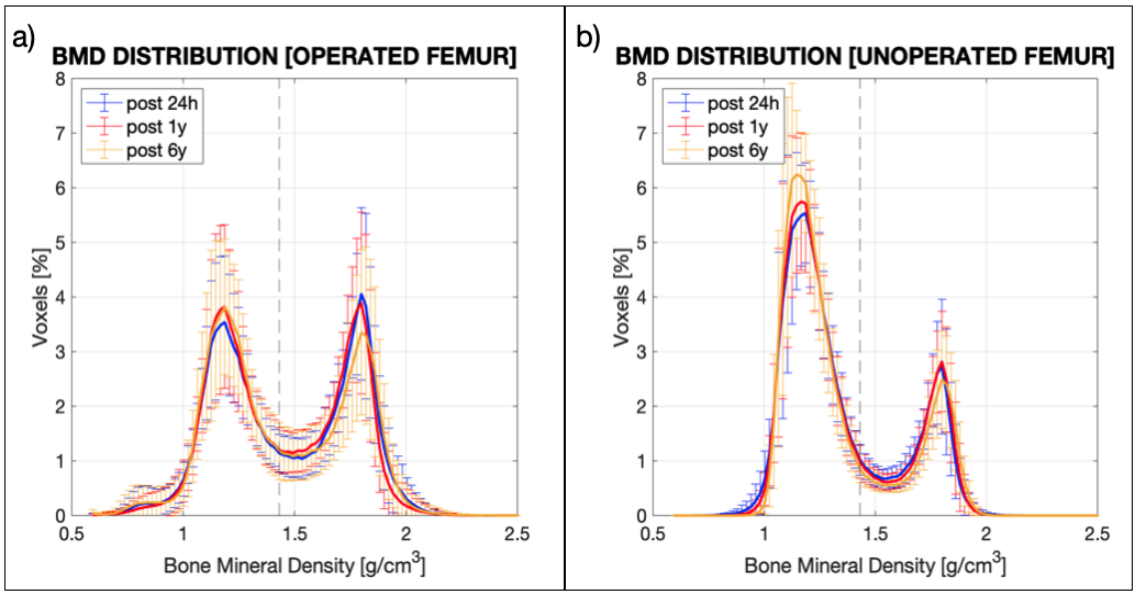

Figure 3.1: Average BMD distribution over the mask of both the operated (a) and unoperated femurs (b). Each point represents the mean and standard deviation of ten patients. The y-axis displays the percentage of voxels at a specific BMD value (x-axis) calculated by eq. 2.2.

For the operated femur, two different analyses were performed to evaluate both the variation in BMD intensity (y-axis) and width (x-axis) respectively.
The first one showed an average increase/decrease rate in both spongeous and cortical bone. The area underlying the curve was calculated for the two types of bone in the three separate datasets, and then values from post 1y and post 6y were normalised by post 24h value using the below formula:

$$Voxel\ frequency\ [\%] = \frac{Area_{Post\ 1y\ (or\ 6y)} - Area_{Post\ 24h}}{Area_{Post\ 24h}} \cdot 100 \qquad (3.1)$$

The three different datasets are reported in abscissa, whereas the ordinate indicates the change in percentage. Average values and standard deviation for both spongeous and cortical bone are shown in figure 3.2.

For the operated femur, a high percentage of spongeous bone was observed over time, reaching a 6.4% raise six years post-operatively. A completely opposite behaviour was observed in cortical bone, since its percentage value decreases up to 6.8% over time. Moreover, post 6y data showed a higher variability than post 1y data, as proven by the greater values of standard deviation (6.7%).

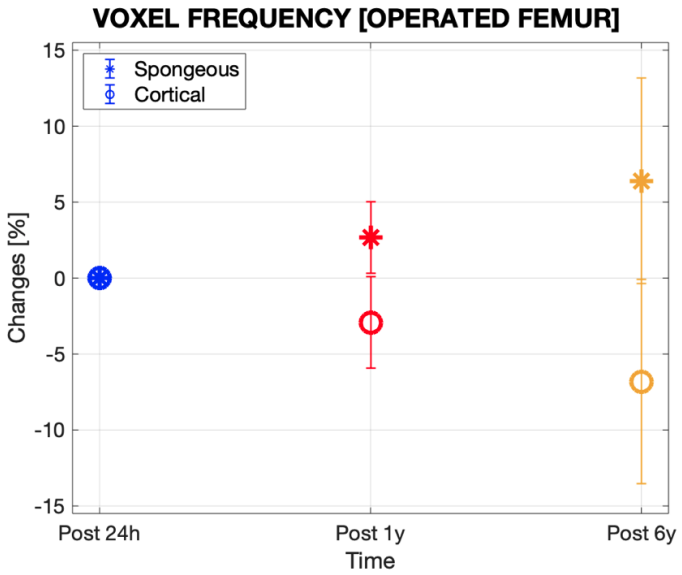

Figure 3.2: Variations [%] in voxel frequency for spongeous and cortical bone over the years (operated femurs). A positive value indicates an increase of frequency of voxels of cortical or spongeous bone.

The second analysis was carried out to assess any average changes in width for both spongeous and cortical BMD. As previously, data were normalised by post 24h value. Table 3.1 reports the average values for each of the ten subjects.
Results showed a great variability among patients. However, the general trend showed no significant change for spongeous bone after one year and six years compared to post 24 hours (respectively -0.078% and -0.235%), while for the cortical bone a slight decrease is measured (respectively -2.951% and -2.724%).

	AVERAGE VALUES - OPERATED FEMUR [g/cm³]			
	$\mu_{\frac{1-24}{24}}[\%]$		$\mu_{\frac{6-24}{24}}[\%]$	
Nº	SPONGEOUS	CORTICAL	SPONGEOUS	CORTICAL
1	0,539	-14,717	-1,387	-13,645
2	-0,312	-0,290	-0,937	0,058
3	-0,157	-4,265	1,178	-7,071
4	0,392	-2,030	-1,177	-0,733
5	0	0	0,080	-2,681
6	0	0,115	0,473	1,094
7	0	-2,198	0,314	-1,954
8	-1,413	-0,522	-0,157	-1,973
9	-0,155	-1,408	-2,405	0,587
10	0,079	-2,074	1,577	1,037
MEAN	-0,078	-2,951	-0,235	-2,724

Table 3.1: BMD average variations [%] for each patient over the years (operated femur). Negative values state for an average loss, positive values for an average gain.

The same two analyses were carried out for the unoperated femur in order to assess any different behaviour compared to the operated leg.
Concerning the bone density variations in voxel frequency (fig. 3.3), no significant changes on average were reported one year after surgery. By looking at the post six years values instead, data showed the same behaviour of the operated femur, with an increase of spongeous bone and a decrease of cortical bone over time. These percentage values are comparable for the latter bony type (-6.2% in the healthy femur instead of -6.8% in the operated one), but a lower increase was observed in the unoperated femur rather than the operated side (2.7% instead of 6.4%).
Regarding average changes in width for both spongeous and cortical BMD in the contra-lateral femur, results showed no relevant changes on average for the spongeous bone for the entire period (-0.087% one year and -0.379% six years post-operatively). No substantial changes were observed for cortical bone too, with just a slight increase of the average value of density six years after undergoing THA (1.038% compared to the post 24h value).

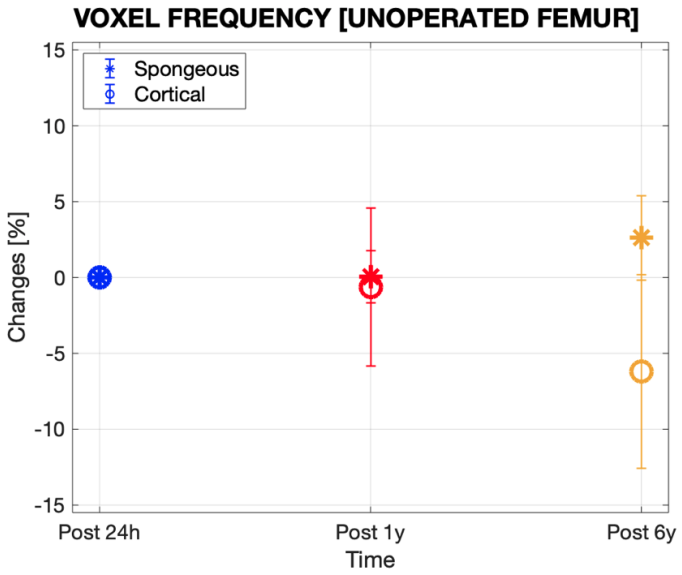

Figure 3.3: Variations [%] in voxel frequency for spongeous and cortical bone over the years (unoperated femur). A positive value indicates an increase of frequency of voxels of cortical or spongeous bone.

	AVERAGE VALUES - UNOPERATED FEMUR [g/cm³]			
	$\mu_{\frac{1-24}{24}}[\%]$		$\mu_{\frac{6-24}{24}}[\%]$	
N°	**SPONGEOUS**	**CORTICAL**	**SPONGEOUS**	**CORTICAL**
1	0,789	0,175	0,237	1,168
2	-0,158	0,868	-1,105	2,199
3	0,080	1,056	0,080	0,939
4	-0,078	0,232	-0,628	-0,348
5	0,079	0	0,159	1,796
6	0	0	-0,318	0,633
7	-0,556	0	-0,238	0,492
8	-0,863	0,708	-1,020	1,535
9	-0,157	0,176	-0,786	1,118
10	0	0,648	-0,157	0,824
MEAN	-0,087	0,387	-0,379	1,038

Table 3.2: BMD average variations [%] for each patient over the years (unoperated femur). Negative values state for an average loss, positive values for an average gain.

Cemented/Uncemented Implants

An analysis on BMD distribution was performed by separating data referred to subjects with a cemented prosthesis from data belonging to patients with an uncemented implant (fig. 3.4). By comparing fig. 3.4,a and fig. 3.4,b, a lower percentage in voxels of spongeous bone was observed in the cemented group (ca 2.5% at the spongeous bone peak) than in the uncemented one (ca 4.0%).
Looking at figure 3.5, a general increase in percentage of voxels for spongeous bone has been observed, reaching +4.8% for subjects with a cemented implant and +7.0% for subjects with an uncemented implant six years post-operation. The cortical bone showed the opposite trend, with a larger decrease in percentage of voxels in the uncemented group (-7.7%) rather than the cemented one (-4.6%).

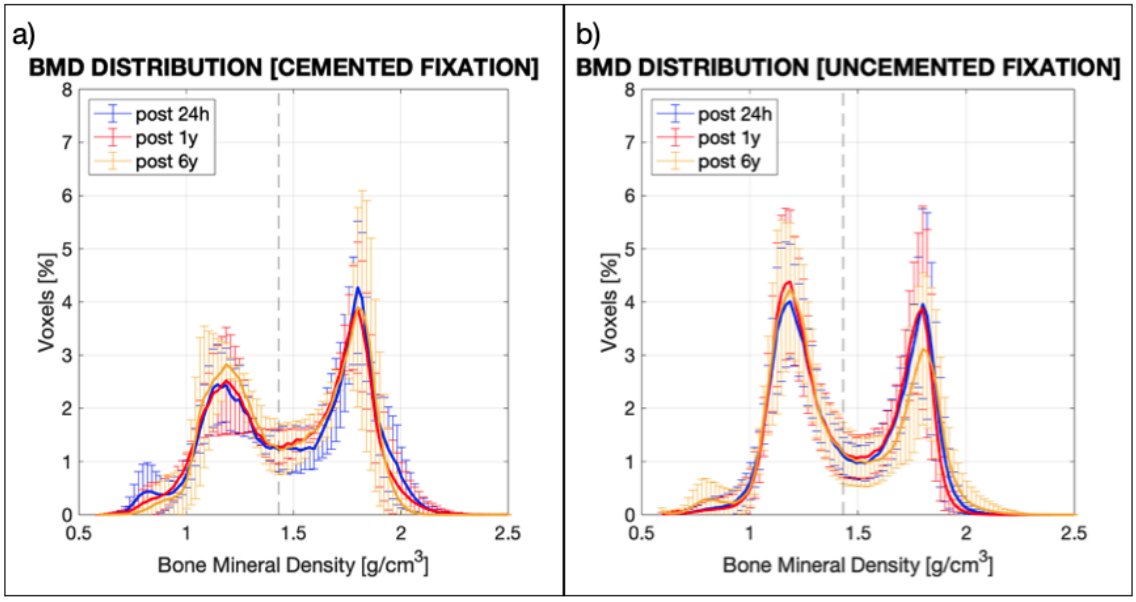

Figure 3.4: Average BMD distribution over the mask of both subjects with a cemented (a) and an uncemented implants (b). Each point represents the mean and standard deviation of ten patients. The y-axis displays the percentage of voxels at a specific BMD value (x-axis) calculated by eq. 2.2.

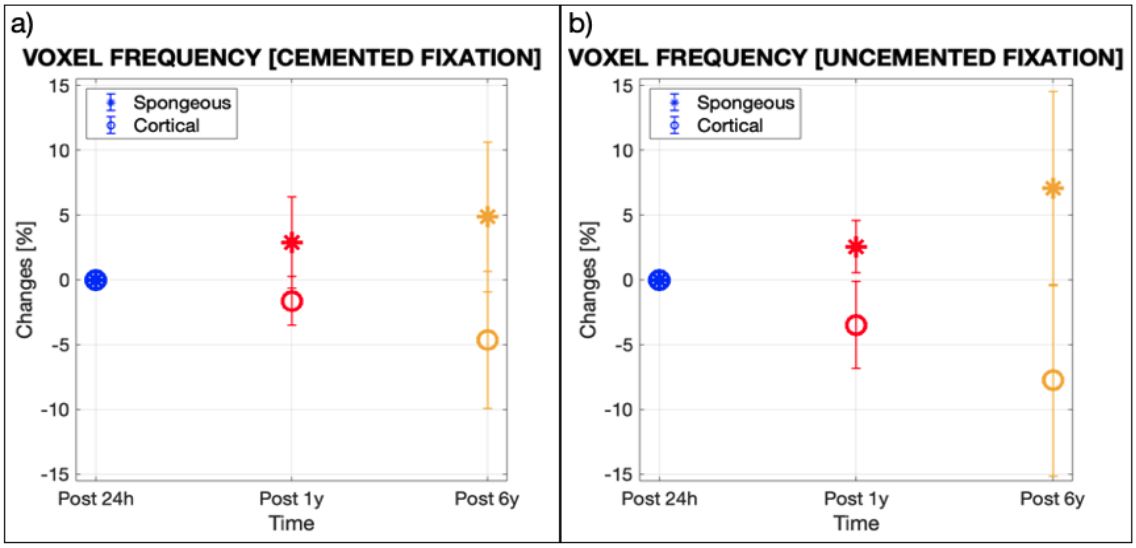

Figure 3.5: Variations [%] in voxel frequency for spongeous and cortical bone over the years in cemented (a) and uncemented fixation (b). A positive value indicates an increase of frequency of voxels of cortical or spongeous bone.

	AVERAGE VALUES - CEMENTED/UNCEMENTED [g/cm³]			
	$\mu_{\frac{1-24}{24}}[\%]$		$\mu_{\frac{6-24}{24}}[\%]$	
	SPONGEOUS	**CORTICAL**	**SPONGEOUS**	**CORTICAL**
MEAN CEM	0,023	-6,424	-0,382	-6,886
MEAN UNCEM	-0,147	-1,384	-0,185	-0,660

Table 3.3: BMD average variations [%] for subjects with cemented and uncemented types of fixation. Negative values state for an average loss, positive values for an average gain.

Moreover, larger standard deviations were observed for uncemented prostheses (± 7.4% for both cortical and spongeous bone) than for cemented ones (± 5.2% for cortical, ± 5.7% for spongeous bone).

Table 3.3 showed average changes in width for spongeous and cortical BMD for these two groups. The greatest loss in average density was noticed for the cortical bone in subjects with a cemented prosthesis (-6.424% one year, -6.886% six years post-operatively).

Female/Male Group

The same analysis approach was performed by separating data according to sex. By observing the BMD distribution for female and male groups (fig. 3.6,a and fig. 3.6,b), a general decrease in voxel frequency for cortical bone is evident, thus confirmed by the negative values in fig. 3.7,a and 3.7,b (-6.7%, -6.9% respectively). In addition, a higher increase in percentage of voxels for the spongeous bone was noticed in women six years after the operation, thus confirmed by a slight average value in fig. 3.7,a (7.2%, instead of 5.6% for men). More significant values for standard deviation were to be noticed for the post 6y data and particularly in the male group, reaching ± 8.9% for the cortical bone (fig. 3.7,b).
However, BMD average variations in width were less substantial when dealing with this group of subjects. Indeed, the greatest density loss was observed in women, with an average value of -4.814% six years after surgery (tab. 3.4).

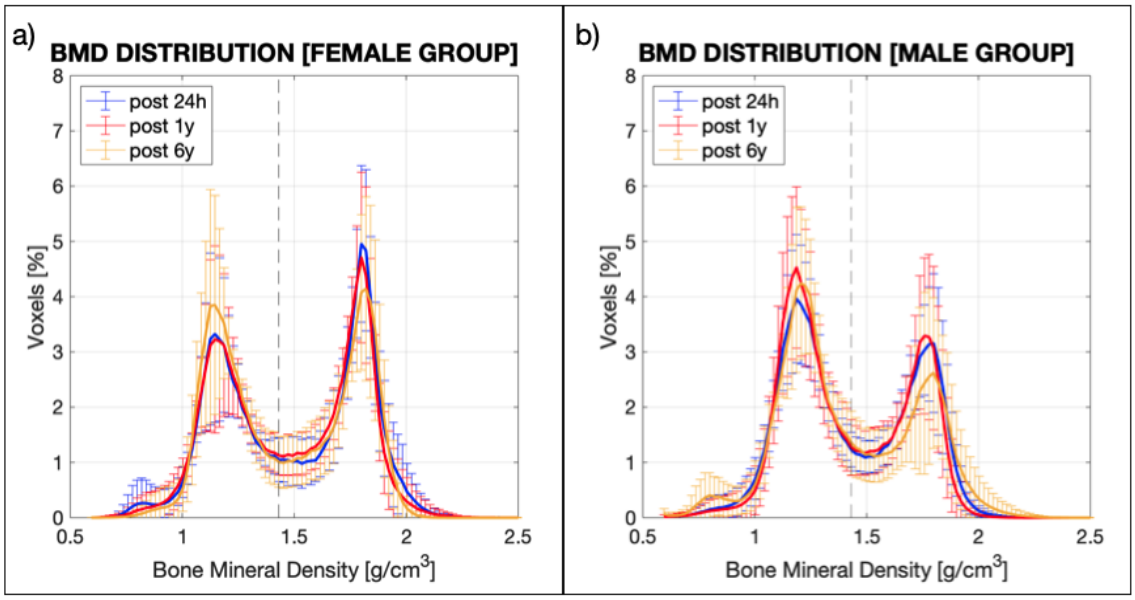

Figure 3.6: Average BMD distribution over the mask of both female (a) and male groups (b). Each point represents the mean and standard deviation of ten patients. The y-axis displays the percentage of voxels at a specific BMD value (x-axis) calculated by eq. 2.2.

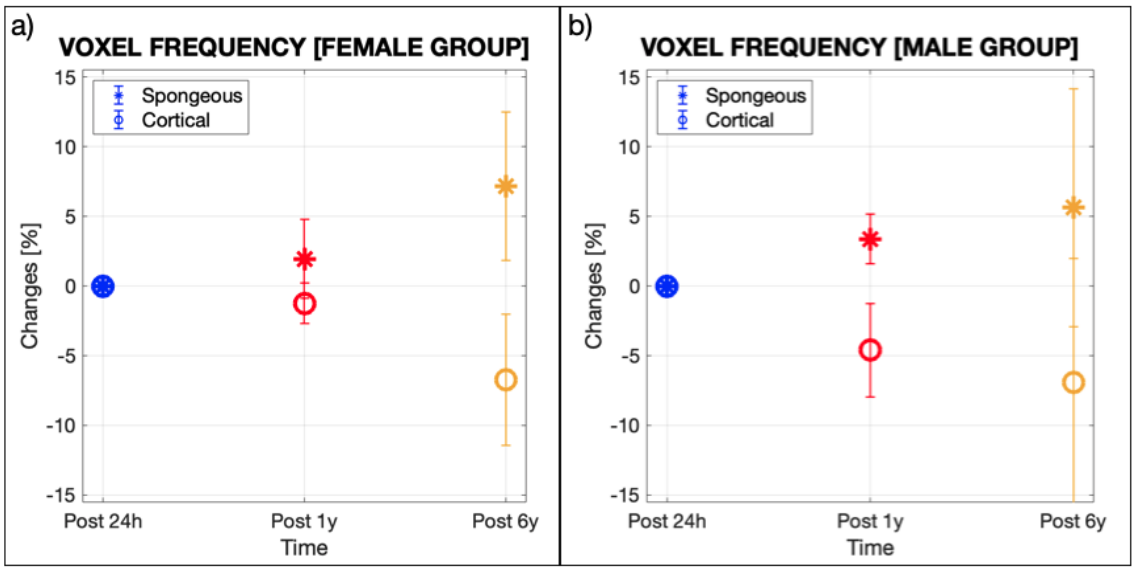

Figure 3.7: Variations [%] in voxel frequency for spongeous and cortical bone over the years for female (a) and male groups (b). A positive value indicates an increase of frequency of voxels of cortical or spongeous bone.

	AVERAGE VALUES - FEMALE/MALE GROUPS [g/cm³]			
	$\mu_{\frac{1-24}{24}}[\%]$		$\mu_{\frac{6-24}{24}}[\%]$	
	SPONGEOUS	**CORTICAL**	**SPONGEOUS**	**CORTICAL**
MEAN FEMALE	0,092	-4,260	-0,449	-4,814
MEAN MALE	-0,298	-1,217	-0,040	-0,242

Table 3.4: BMD average variations [%] for female and male groups. Negative values state for an average loss, positive values for an average gain.

3.2 BMD Evaluation in Gruen Zones

Bone remodelling has also been investigated in the seven Gruen zones, in order to better locate where the most significant changes occur.

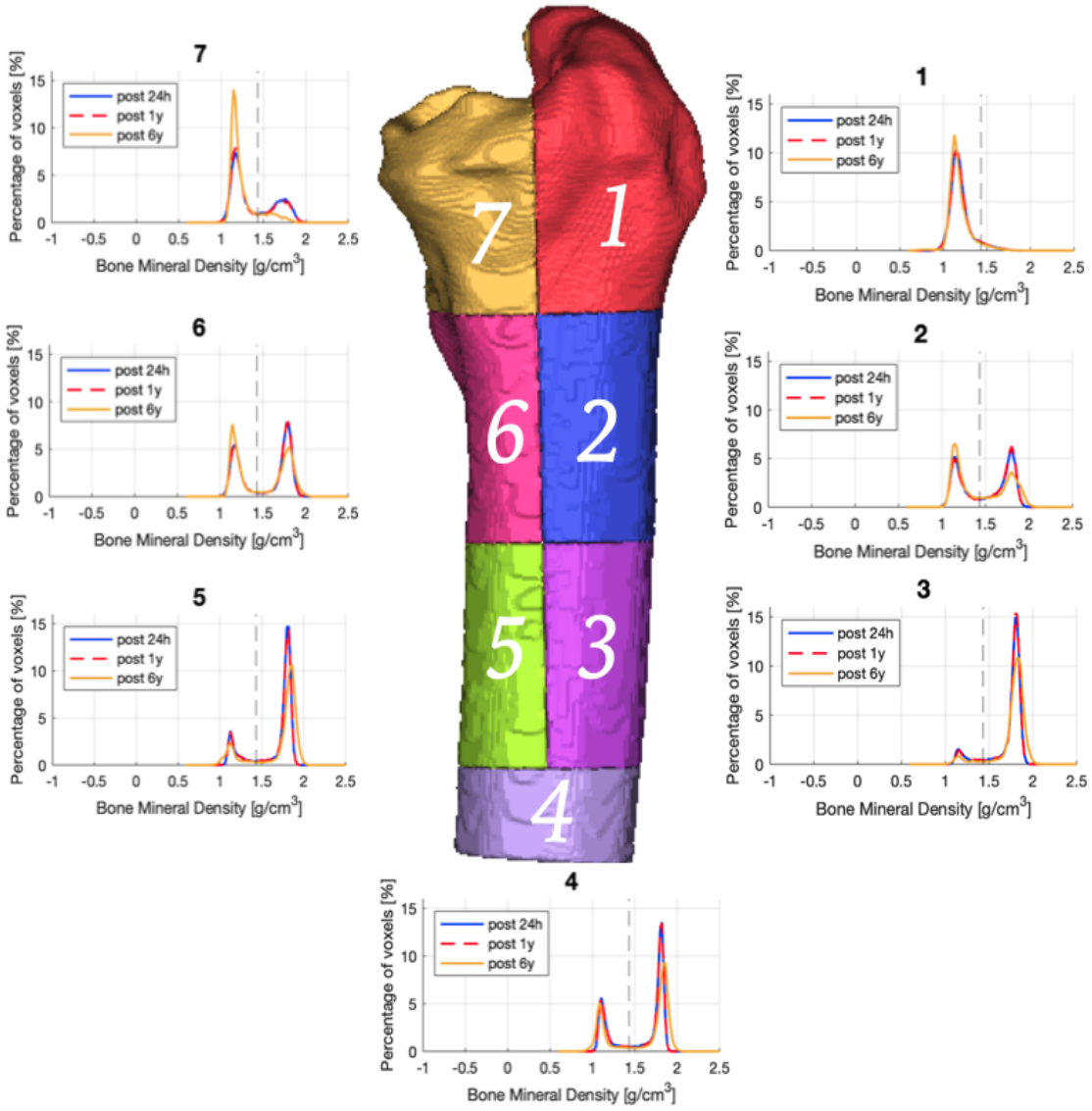

Figure 3.8: BMD distributions for the seven Gruen zones.

Operated/Unoperated Femur

Figure 3.9,a shows BMD mean changes in voxel frequency for both spongeous and cortical bone in every Gruen zone for the operated femur. The most significant decrease rate for cortical bone was observed in Gruen zones 1, 2, 6 and 7 after six years (-5.4%, -7.1%, -8.4%, and -16.3% respectively). Minor changes for cortical bone were observed in areas 3, 4, 5 (-3.2%, -2.7%, and 0.4% respectively).

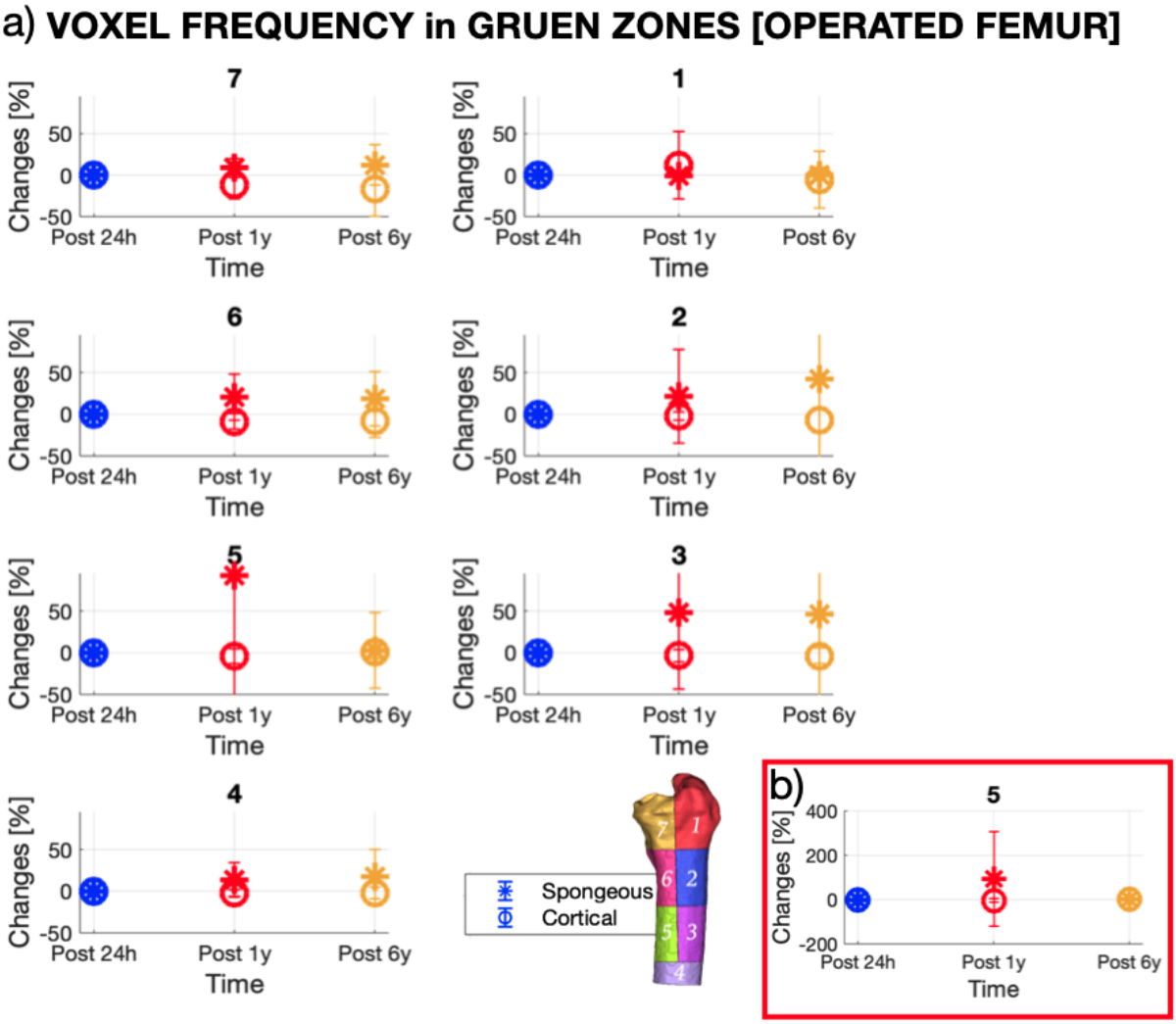

Figure 3.9: a) Variations [%] in voxel frequency for spongeous and cortical bone in the seven Gruen zones over the years (operated femurs). To better assess any change, y-axis limit is set to [-50 95]. b) Variations [%] in voxel frequency for zone 5 shown with no y-axis limit.

Concerning the spongeous bone, the highest increase in percentage was located in areas 2 and 3 (42.6% and 46.0% respectively) six years post-operatively. A high increment was located also in area 5 one year after surgery (92.4%), but after six year the increase rate was just 3.5% if comparing post 6y data with post 24h ones. In addition, the variability among patients in this area was really significant, reaching as far a standard deviation of ± 213% in area 5 (fig. 3.9,b).
Regarding the average values of bone mineral density (tab. 3.5), an initial bone loss in density occurred in all zones except for the first one. Six years post-operatively, a decrease in BMD occurred just for Gruen zones 1 and 2. All the other areas showed an increase, especially in the fifth zone (2.766%).

AVERAGE VALUES IN GRUEN ZONES - OPERATED FEMUR [g/cm³]		
GRUEN ZONE	$\mu_{\frac{1-24}{24}}[\%]$	$\mu_{\frac{6-1}{1}}[\%]$
1	1,019	-1,189
2	-1,539	-0,605
3	-2,103	0,997
4	-0,960	0,847
5	-2,060	2,766
6	-2,824	0,916
7	-1,902	0,277

Table 3.5: BMD average variations [%] in each Gruen zone (operated femurs). Post 1y data are normalised by post 24h data, while post 6y data are normalised by post 1y ones to better assess any change from the previous dataset. Negative values state for an average loss, positive values for an average gain.

Fig. 3.10 shows the BMD variation of each Gruen zone for the unoperated femur. As observed for the operated dataset, proximal areas (1, 2, 6, and 7) had the most relevant decrease of cortical bone over time (-13.9%, -7.1%, -8.5%, and -9.9% respectively six years after surgery), whereas the most important increase in spongeous bone was observed in Gruen zone 5 (21.3% six years post-operatively).

Concerning the average value of mineral density (tab. 3.6), a slight increase in the contralateral leg values occurred in zones 1, 5, 6 and 7 after one year. However, the general trend after 6 years was a decrease for all of them, especially in Gruen zone 6 (-1.945%).

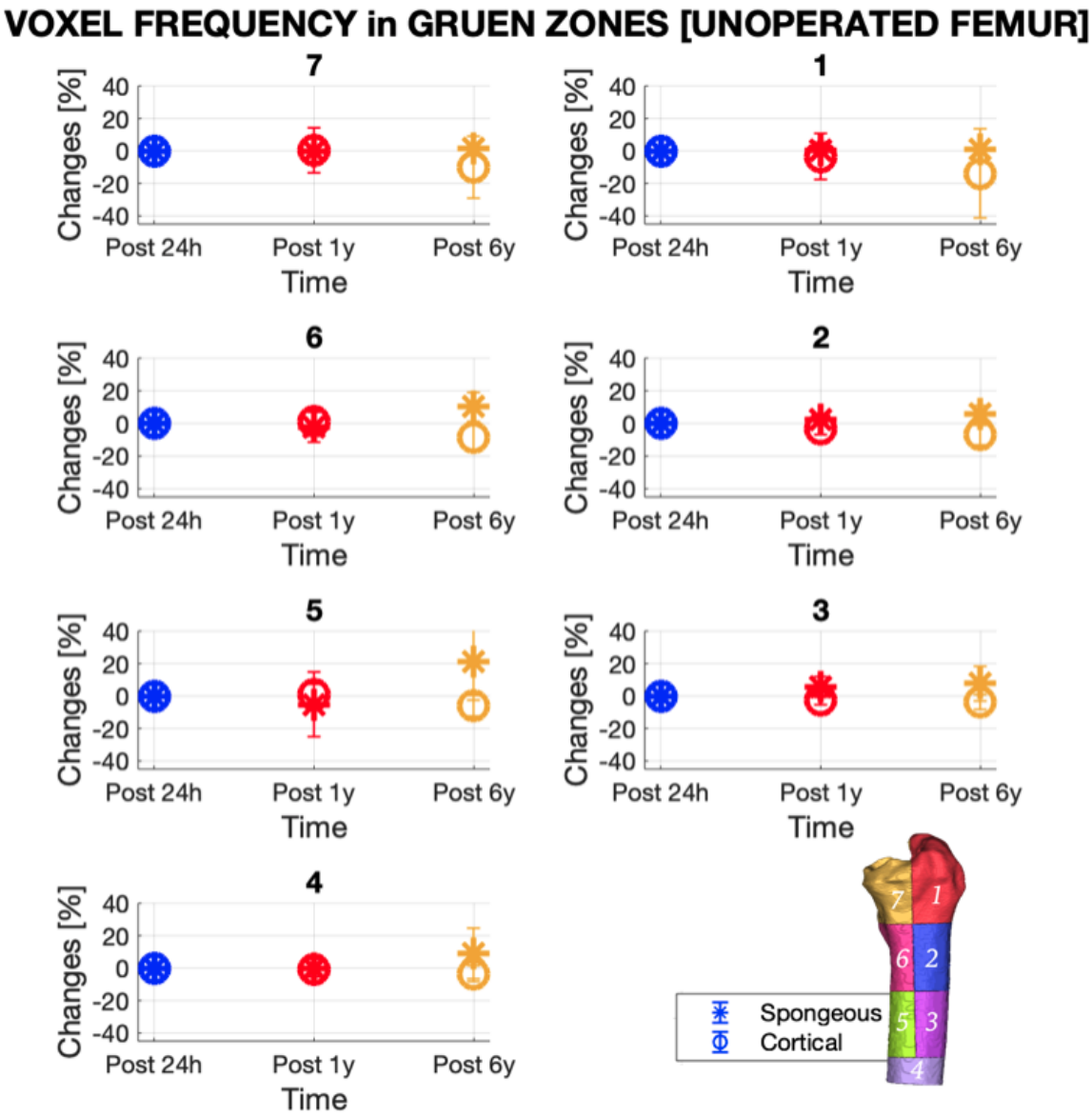

Figure 3.10: Variations [%] in voxel frequency for spongeous and cortical bone in the seven Gruen zones over the years (unoperated femurs). To better assess any change, y-axis limit is set to [-45 40].

AVERAGE VALUES IN GRUEN ZONES - UNOPERATED FEMUR [g/cm³]		
GRUEN ZONE	$\mu_{\frac{1-24}{24}}[\%]$	$\mu_{\frac{6-1}{1}}[\%]$
1	0,075	-0,253
2	-0,349	-0,690
3	-0,410	-0,008
4	0,269	-0,370
5	0,784	-1,572
6	0,663	-1,945
7	0,199	-0,314

Table 3.6: BMD average variations [%] in each Gruen zone (unoperated femurs). Post 1y data are normalised by post 24h data, while post 6y data are normalised by post 1y ones. Negative values state for an average loss, positive values for an average gain.

Cemented/Uncemented Implants

By observing fig. 3.11 and fig. 3.12, the general trend of reduction of cortical bone was noticed for both types of fixation. For the cemented group, an increase in percentage for spongeous bone was observed in Gruen zone 3 and 4 (104.5%, 61.0% respectively). For the uncemented group, a raise for spongy bone was noted in area 5 one year after surgery (134.8%), followed by a reduction that resulted in an increased rate of just 17.2% six years post-operatively. In this zone, the greatest values for standard deviation occurred for the post 1y dataset (± 247.5%), along with Gruen zone 3 (± 106.4%).
Looking at tab. 3.7 and tab. 3.8, a higher loss in percentage occurred for areas 3, 4, 5, 6, 7 in the uncemented fixation rather than the cemented type one year post-operation. However, after six years, in all these Gruen zones a higher gain was observed in the former, in contrast with a loss for areas 2 and 3 for the cemented type. A turnaround can be seen for area 1, wherein a gain in average density was visible in the cemented type of fixation.

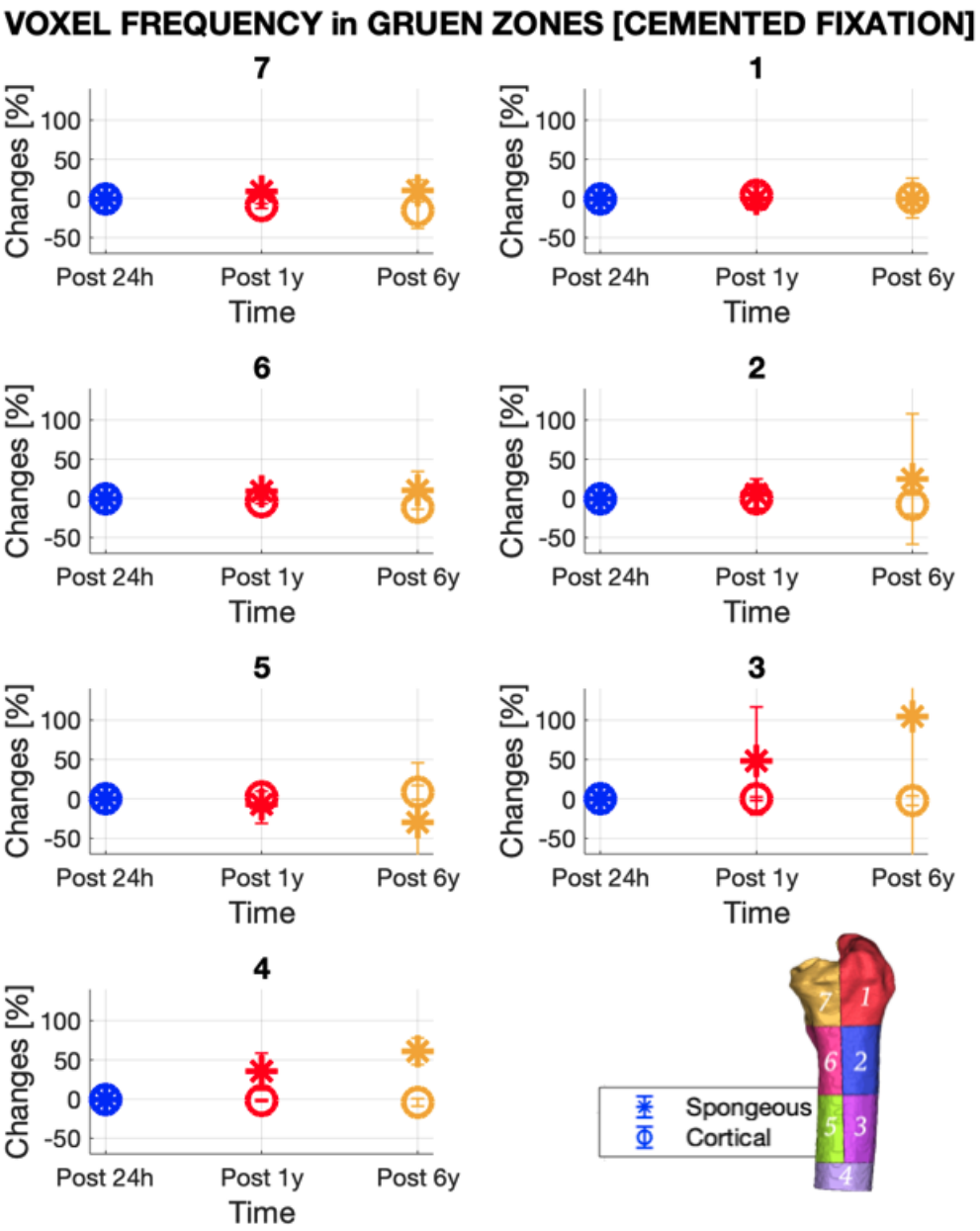

Figure 3.11: Variations [%] in voxel frequency for spongeous and cortical bone in the seven Gruen zones over the years (cemented group). To better assess any change, y-axis limit is set to [-70 140].

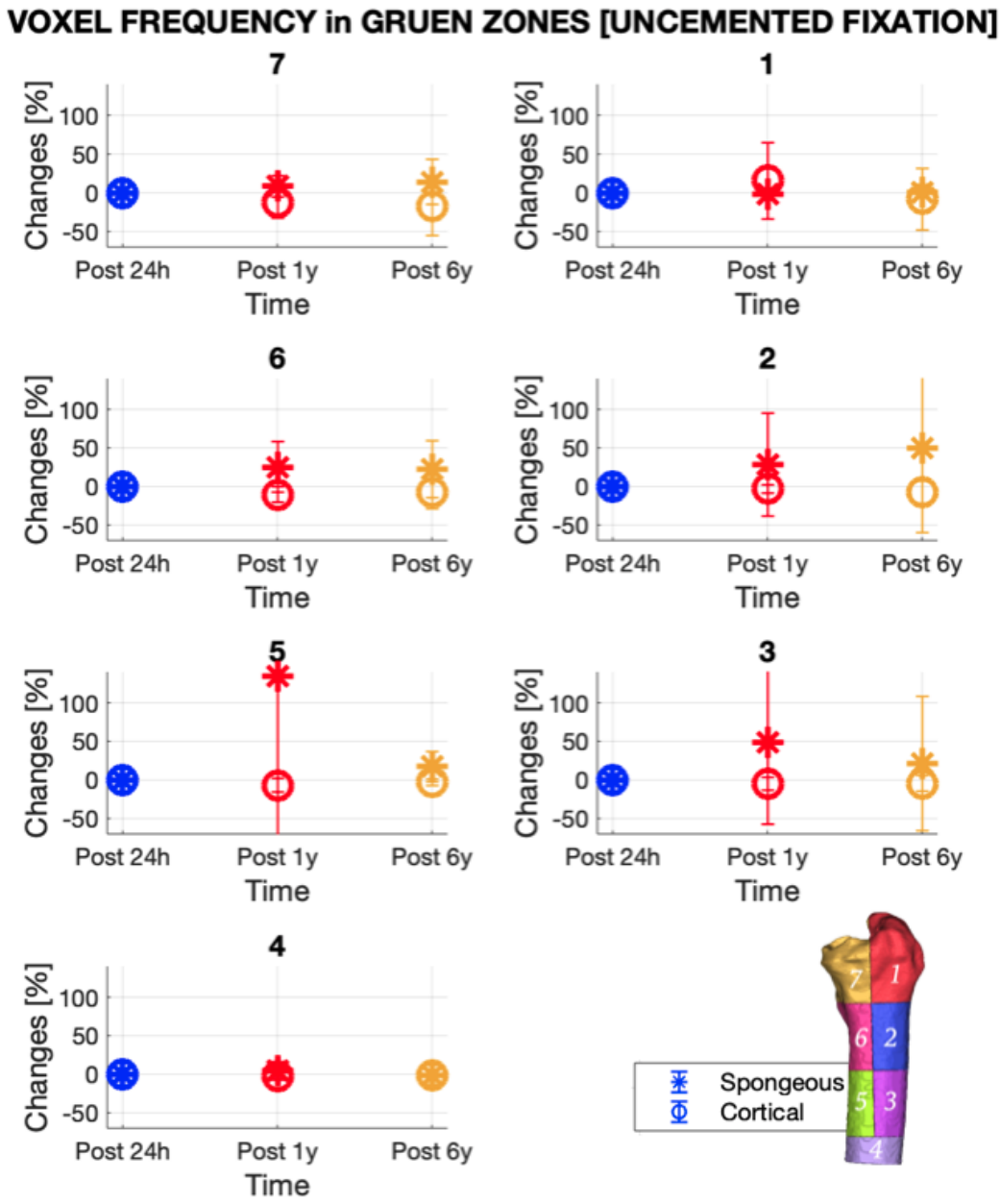

Figure 3.12: Variations [%] in voxel frequency for spongeous and cortical bone in the seven Gruen zones over the years (uncemented group). To better assess any change, y-axis limit is set to [-70 140].

AVERAGE VALUES IN GRUEN ZONES - CEMENTED FIXATION [g/cm³]		
GRUEN ZONE	$\mu_{\frac{1-24}{24}}[\%]$	$\mu_{\frac{6-1}{1}}[\%]$
1	1,011	0,957
2	-1,847	-2,298
3	-2,000	-0,799
4	-0,748	0,487
5	-0,401	1,533
6	-1,731	-1,252
7	-1,049	0,701

Table 3.7: BMD average variations [%] in each Gruen zone (cemented group). Post 1y data are normalised by post 24h data, while post 6y data are normalised by post 1y ones to better assess any change from the previous dataset. Negative values state for an average loss, positive values for an average gain.

AVERAGE VALUES IN GRUEN ZONES - UNCEMENTED FIXATION [g/cm³]		
GRUEN ZONE	$\mu_{\frac{1-24}{24}}[\%]$	$\mu_{\frac{6-1}{1}}[\%]$
1	1,022	-2,109
2	-1,407	0,120
3	-2,147	1,767
4	-1,051	1,002
5	-2,771	3,294
6	-3,292	1,845
7	-2,267	0,095

Table 3.8: BMD average variations [%] in each Gruen zone (uncemented group). Post 1y data are normalised by post 24h data, while post 6y data are normalised by post 1y ones to better assess any change from the previous dataset. Negative values state for an average loss, positive values for an average gain.

Female/Male Group

Fig. 3.13 and fig. 3.14 show voxel frequencies [%] divided by sex groups. Both groups exhibited the general trend of reduction for cortical bone in Gruen zones 1, 2, 6, and 7 shown previously, along with an increase for spongeous bone particularly evident for area 2 in the women's cohort (77.8%).

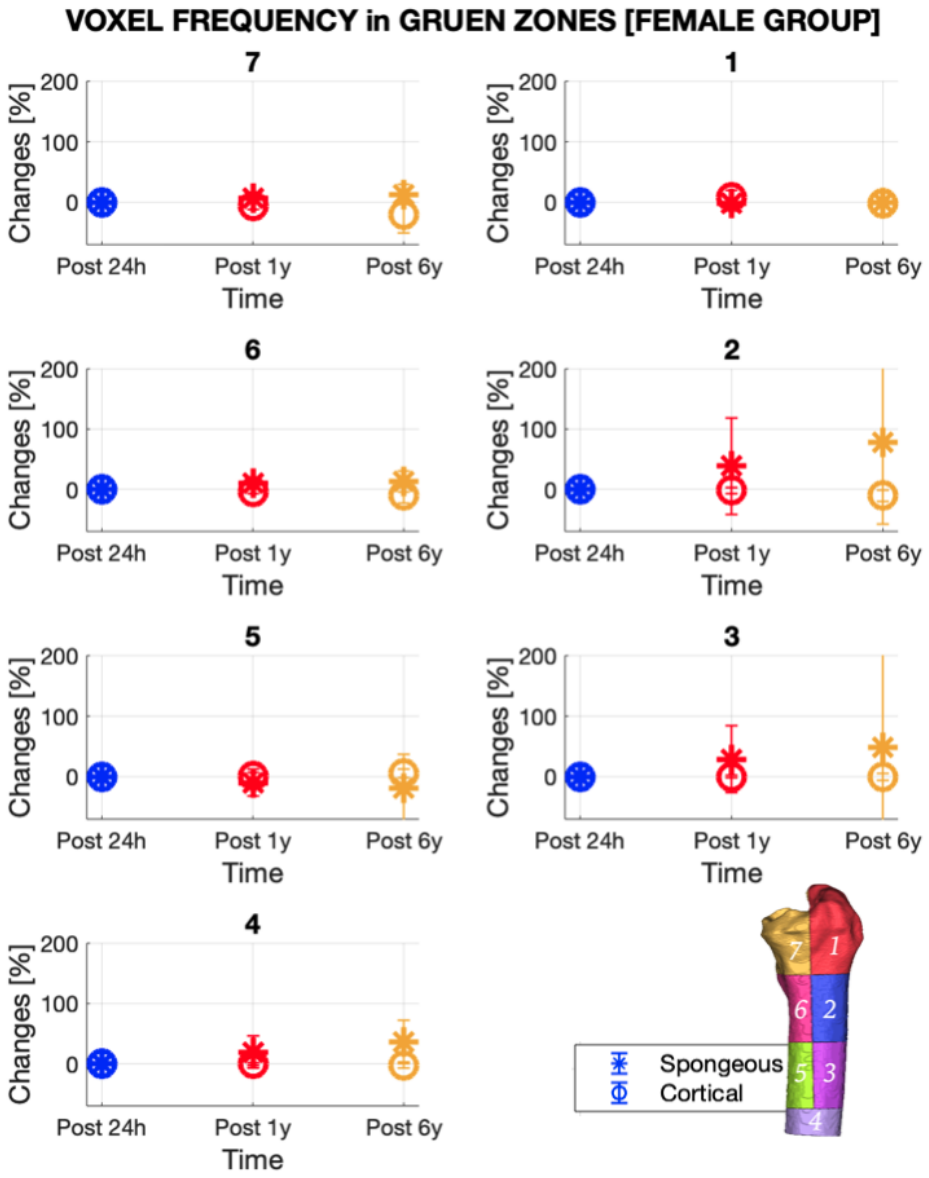

Figure 3.13: Variations [%] in voxel frequency for spongeous and cortical bone in the seven Gruen zones over the years (female group). To better compare any change with the male group, y-axis limit is set to [-70 200].

Post 6y data in Gruen zones 2 and 3 show a greater variability for the female group compared to the male one, with a standard deviation reaching as far as ± 189% in area 3. By contrast, post 1y data in areas 3 and 5 show a larger variability in men's cohort, reaching as far a standard deviation of ± 275% in area 5 (fig. 3.14).

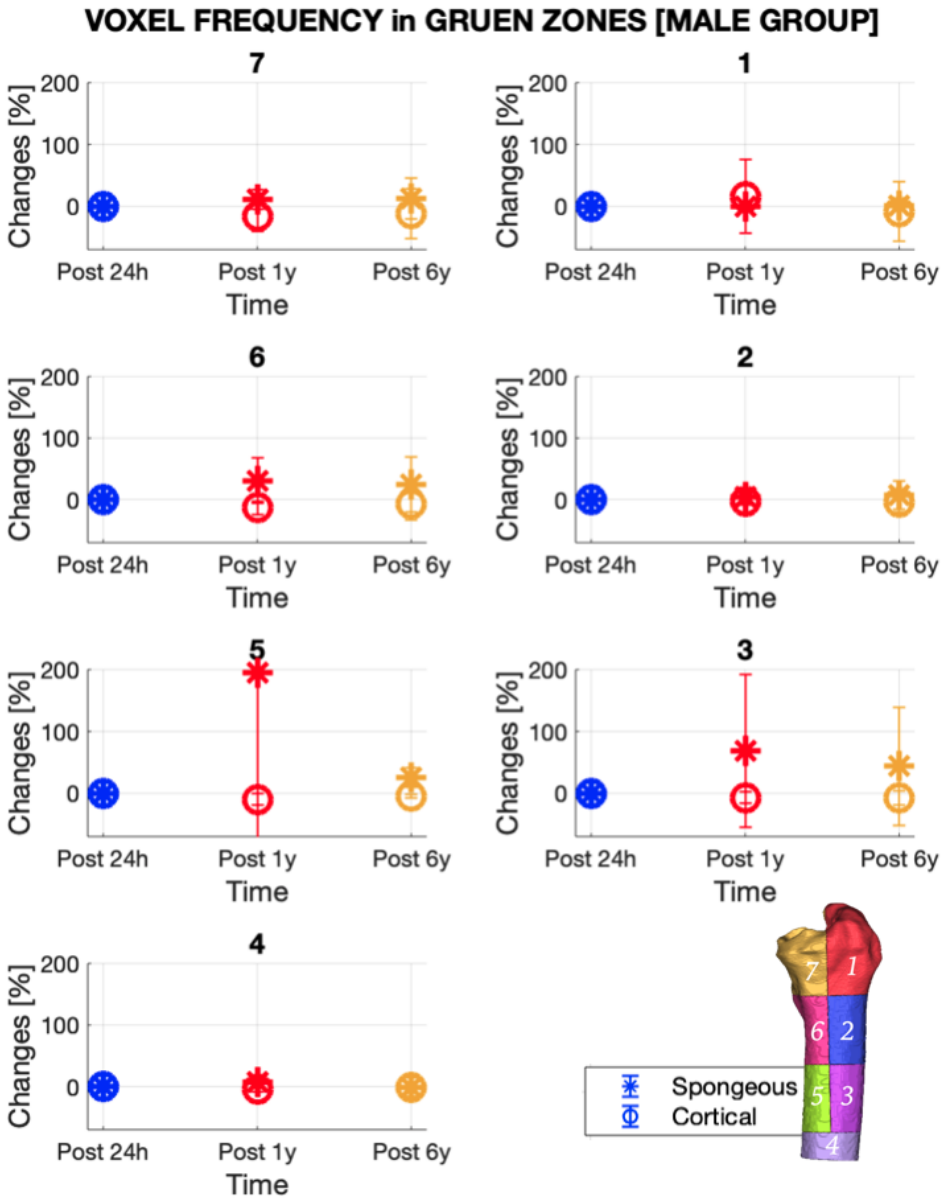

Figure 3.14: Variations [%] in voxel frequency for spongeous and cortical bone in the seven Gruen zones over the years (male group). To better compare any change with the female group, y-axis limit is set to [-70 200].

AVERAGE VALUES IN GRUEN ZONES - FEMALE GROUP [g/cm³]		
GRUEN ZONE	$\mu_{\frac{1-24}{24}}[\%]$	$\mu_{\frac{6-1}{1}}[\%]$
1	0,920	-0,041
2	-1,870	-2,209
3	-1,508	0,237
4	-0,542	0,556
5	-0,537	1,751
6	-1,750	-0,944
7	-0,944	-1,355

Table 3.9: BMD average variations [%] in each Gruen zone (female group). Post 1y data are normalised by post 24h data, while post 6y data are normalised by post 1y ones to better assess any change from the previous dataset. Negative values state for an average loss, positive values for an average gain.

AVERAGE VALUES IN GRUEN ZONES - MALE GROUP [g/cm³]		
GRUEN ZONE	$\mu_{\frac{1-24}{24}}[\%]$	$\mu_{\frac{6-1}{1}}[\%]$
1	1,118	-2,337
2	-1,208	0,998
3	-2,698	1,756
4	-1,379	1,138
5	-3,583	3,781
6	-3,898	2,776
7	-2,860	1,909

Table 3.10: BMD average variations [%] in each Gruen zone (male group). Post 1y data are normalised by post 24h data, while post 6y data are normalised by post 1y ones to better assess any change from the previous dataset. Negative values state for an average loss, positive values for an average gain.

By observing the average BMD values for each Gruen zone in tab. 3.9 and tab. 3.10, men had a higher loss in percentage in areas 3, 4, 5, 6, 7 than women one year post-operatively. That is particularly evident in area 6, where there is a loss of -3.898% for the male group. However, in men's cohort a gain was observed in all these Gruen zones (except for area 1) after six years. In women's group, just the average values from areas 3, 4, and 5 showed a gain compared to post 24h data.

3.3 New Bone Formations

Fig. 3.15, 3.16, 3.17, and 3.18 show four examples obtained after performing "part comparison analysis" in 3Matic to better localise where new bony formations occurred. To get an overview of all the different groups, the first subject was selected from the "female cemented" cohort, the second patient from the "female uncemented" cohort, while the third and fourth subjects from the "male uncemented" one.

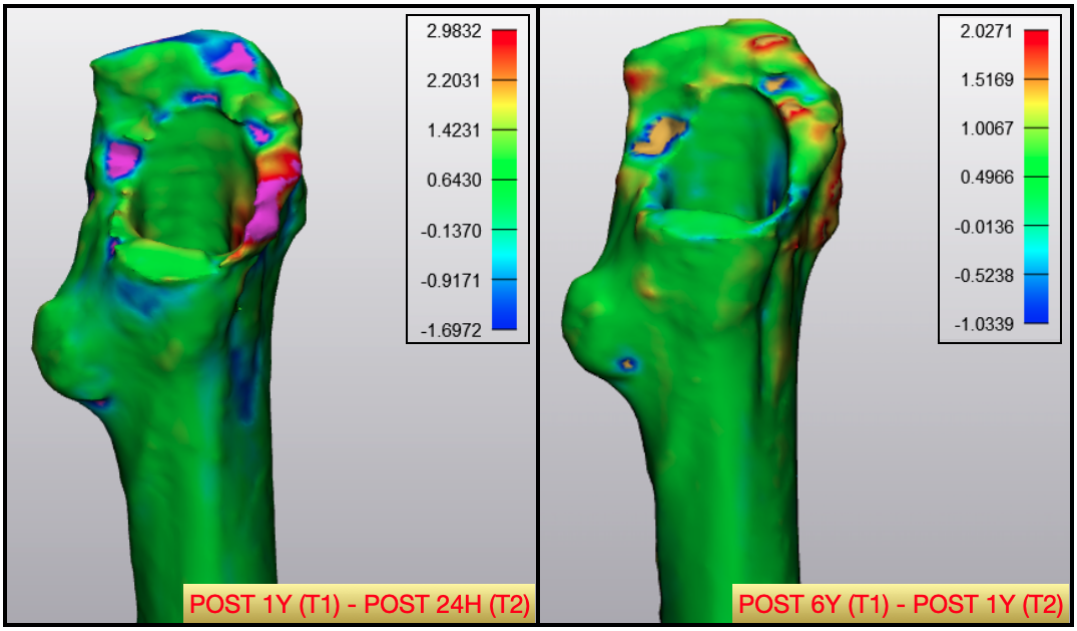

Figure 3.15: "Part comparison analysis" between post 24h and post 1y masks (on the left) and post 1y and post 6y masks (on the right) from a female with a cemented prosthesis. The colormaps state for the maximum and the minimum distance reached for each comparison.

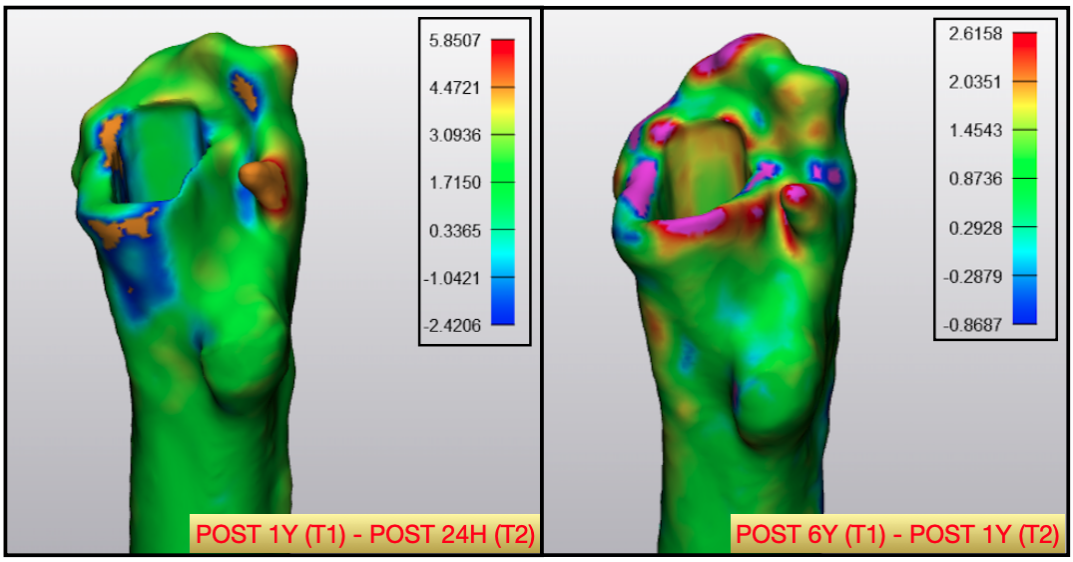

Figure 3.16: "Part comparison analysis" between post 24h and post 1y masks (on the left) and post 1y and post 6y masks (on the right) from a female with an uncemented prosthesis. The colormaps state for the maximum and the minimum distance reached for each comparison.

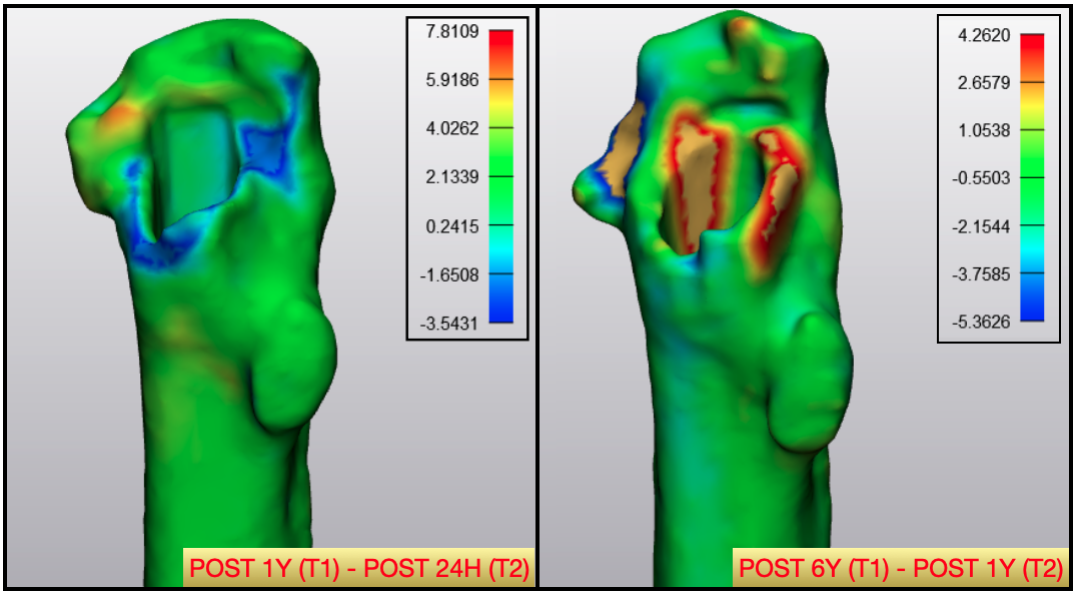

Figure 3.17: "Part comparison analysis" between post 24h and post 1y masks (on the left) and post 1y and post 6y masks (on the right) from a male with a uncemented prosthesis. The colormaps state for the maximum and the minimum distance reached for each comparison.

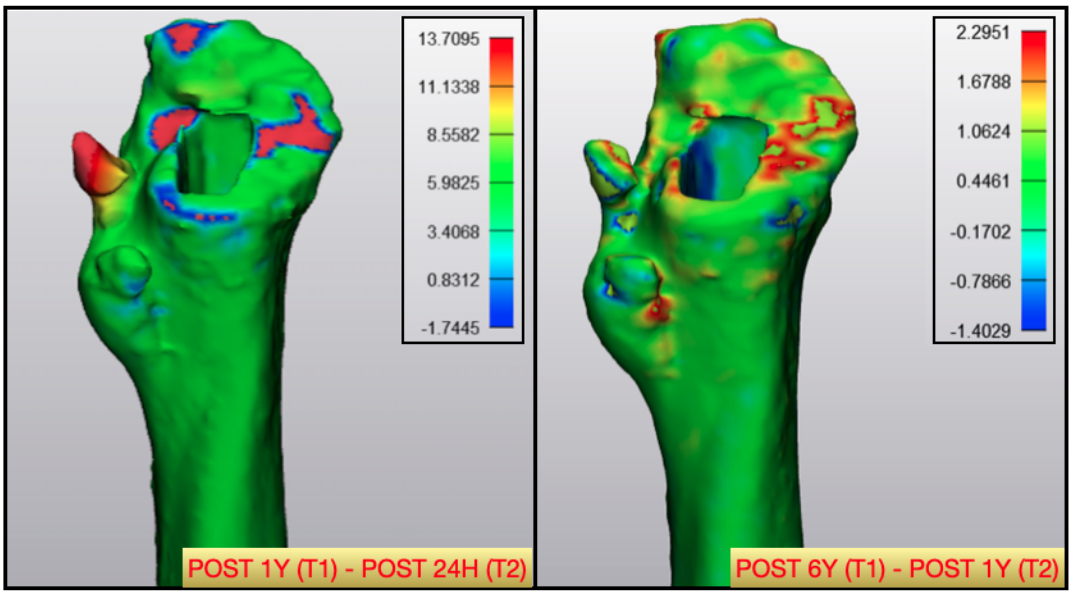

Figure 3.18: "Part comparison analysis" between post 24h and post 1y masks (on the left) and post 1y and post 6y masks (on the right) from a male with an uncemented prosthesis. The colormaps state for the maximum and the minimum distance reached for each comparison.

By looking at the bottom three figures, a bone resorption occurred in the proximal area of the femur one year after surgery for patients with an uncemented implant. No other similar behaviours were to be noted over the years.

Chapter 4

Discussion

This work is only a part of a broader project that stems from the collaboration between Landspitali – University Hospital of Iceland and the Institute for Biomedical and Neural Engineering of Reykjavík University. The final aim is to establish a clinical evaluation score for total hip replacement planning and for post-operative assessment, since currently orthopedic surgeons do not have any quantitative guideline for selecting the optimal implant, and they just rely on their experience and some qualitative evaluations for the choice.
The purpose of this study was to create a feasible and repeatable protocol to evaluate the three-dimensional changes of bone mineral density in both the operated and the contra-lateral femur, giving a qualitative and quantitative assessment on how much bone's volume has increased/decreased and how bone quality has changed one year and six/seven years post-operatively. Through this protocol, BMD changes were also evaluated separately in the seven standard Gruen zones. Furthermore, an assessment of where bony formations/resorptions are to occur was provided. Results have been reported so as to compare respectively:

- the operated/unoperated femurs;
- the cemented/uncemented groups;
- the female/male groups;

In such manner, any different behaviour emerging from these categories could be investigated over time.

As already mentioned in the previous chapter, results show a great variations among subjects. This is due to the inter-patient variability. Indeed, study participants differ in sex, age, lifestyle, surgical approach, other than for the type of implant inserted. The limited number of subjects involved in the study allows the estimation of a general trend among the different categories (e.g. cemented/uncemented), trend that will be discussed below. However, only the evaluation of a wider patients' cohort will give the opportunity to draw final conclusions.

4.1 Bone Mineral Density Changes

Concerning the BMD distributions, the lower amount of spongeous bone that occurred in the operated side rather than the unoperated side (fig. 3.1) is caused by the removal of bone due to the arthroplasty. Indeed, most of the bone rasped away to create the intra-medullary cavity to place the stem consists in spongeous bone. Moreover, the amount of bone removed was greater in the cemented group compared to the uncemented one, since a larger hollow is required to place the cement. This explains why a lower percentage of spongeous bone was observed in the BMD distribution of the cemented group (fig. 3.4) as well as in the female group (fig. 3.6), consisting of both subjects with a cemented/uncemented type of fixation.

Regarding the voxel frequency analysis, a general trend was observed for all these groups, with an increase in percentage for the spongeous bone and a decrease for the cortical one six years after THA (figs. 3.2, 3.3, 3.5, and 3.7). Such results are consistent with literature, and in particular with the bone remodeling process that takes place after the age of 40. Indeed, a great portion of the resorption occurs along the endocortical surface, where the spongeous bone seems to replace the cortical bone, building a framework which supplies large surfaces to rapidly provide minerals and different cell types and their progenitors [77, 78].

Concerning average changes in width for both spongeous and cortical BMD, no significant changes were to be noted for the spongeous bone. Instead, the average value of the cortical bone showed a decrease that was more pronounced in the cemented group than the uncemented one six years post-operatively (tabs. 3.1 and 3.3). This outcome confirms that uncemented implants have better performances

than cemented ones in a long-term scenario. Such information (and particularly the percentage rate) should be taken into account by different specialists (e.g. physiotherapists) to develop the best strategy in terms of rehabilitation and postural control as early as one year post-operation. The following assessment seeks to supply a better quality of life for the patients, trying to reduce the need for a revision surgery.

4.2 BMD Evaluation in Gruen Zones

The analysis carried out by evaluating separately each Gruen zone proved a general trend of percentage decrease for cortical bone in areas 1, 2, 6, and 7 (figs. 3.9 – 3.14). This result is consistent with literature, since the highest bone loss is expected to occur in the proximal area of the femur. Instead, Gruen zones 3 and 5 showed the highest increase in percentage for spongeous bone. However, these two areas were the ones most affected by variability among patients, especially for the uncemented category (and thus indirectly for the men's cohort, since most of the subjects with an uncemented implant was men). A possible explanation lies in the surgical procedure of the press-fit method. Indeed, the femoral canal has to be rasped away in order to place the stem. When performing this task, surgeons do their best to create a hollow that is centered on the longitudinal axis of the femur. However, even a small change in angle can cause a significant change in voxel frequency, given that such areas have a smaller volume compare to the others.

Regarding the average values of bone mineral density in the operated femurs, the initial bone loss observed for all the zones (except for 1) is mainly due to the mechanism of bony riadjustment after the removal of a consistent part of the bone (tab. 3.5). However, the general trend after six years varies depending on the type of implant. As shown in tabs. 3.7 and 3.8, a loss for areas 2, 3, and 6 was observed for the cemented group. Such outcome is caused by a problem of pressure. Indeed, while inserting the cement, the areas affected by the largest pressure are zone 3, 4, and 5. By placing the prosthesis inside the cavity, the surgeon has to apply a certain strength to drive up the cement. Depending on this level of strength, a certain pressure will be reached even in areas 2 and 6. The lesser it is, the less the

bone receives a mechanical stress at the prosthesis/bone interface, causing a loss in the average BMD value.
Concerning the uncemented group, a gain in density was noticed in all Gruen zones six years post-operatively, except for zone 1. Indeed, with the uncemented approach a larger region of bone is removed from this area rather the cemented technique. Such outcome is achieved to ensure a good alignment with the longitudinal axis of the femur when the prosthesis has to be inserted in the intra-medullary cavity. However, this operation entails a lower stimulation in the proximal part of the femur, leading to a greater chance to cause a BMD loss in this area.
By looking at female/male groups separately (tabs. 3.9 and 3.10), such analysis added no relevant information as compared to the cemented/uncemented one. However, further information on clinical data may give insights on the search for correlations between some pathologies (e.g. osteoporosis) and the bone remodelling in specific areas.
Even in this case, information about the bone remodelling in the different areas could provide a successful tool to develop specific rehabilitation strategies to allow the patients to have a healthy lifestyle, trying to avoid successive surgeries.

4.3 New Bone Formations

Through the results obtained to evaluate any bone formation/resorption, it is only fair to affirm that a bone resorption occurred in the proximal area of the femur one year post-operation, since no other similar behaviours were observed. However, a landmark registration was used to pre-align the masks, so that the accuracy by which this operation is performed relies significantly on the operator's hand. To overcome such issue, another work in the wider THA project was focused on the development of an algorithm to perform a totally automatic registration. By using this tool, a more accurate 3-dimensional analysis of where bone gain and loss occur can be conducted, avoiding recurring issues caused by intra- and inter-operator variability.
An example of 3D bone remodelling from the "female cemented" cohort and from the "male uncemented" one is given below (figs. 4.1 – 4.4).

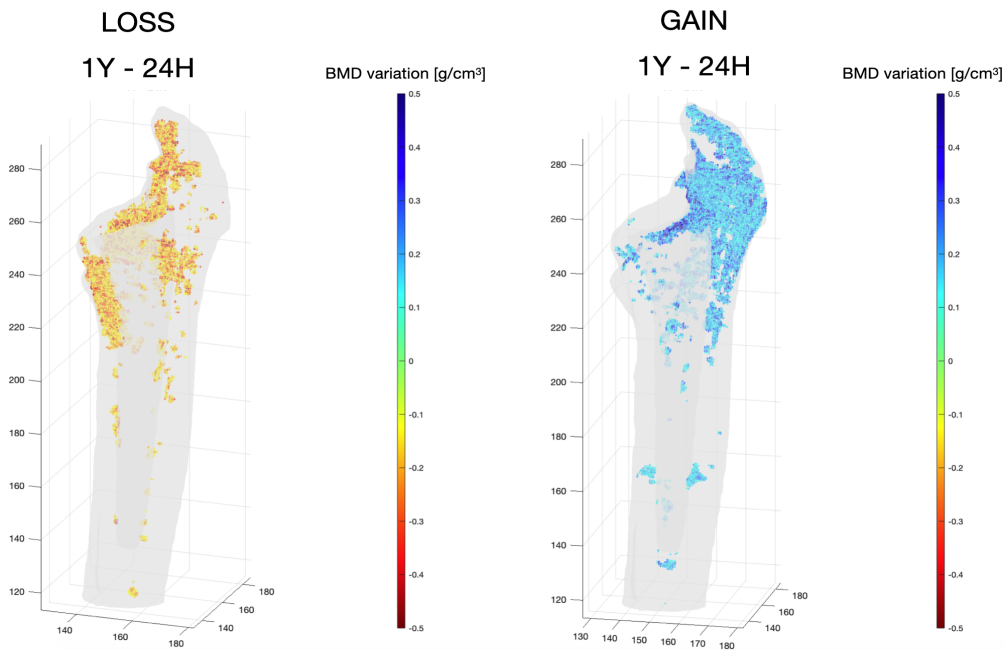

Figure 4.1: 3D BMD evaluation one year post-operation (female cemented). Blue points states for a gain, orange ones for a loss. The threshold was set at $\pm$ 0.1 g/cm^3.

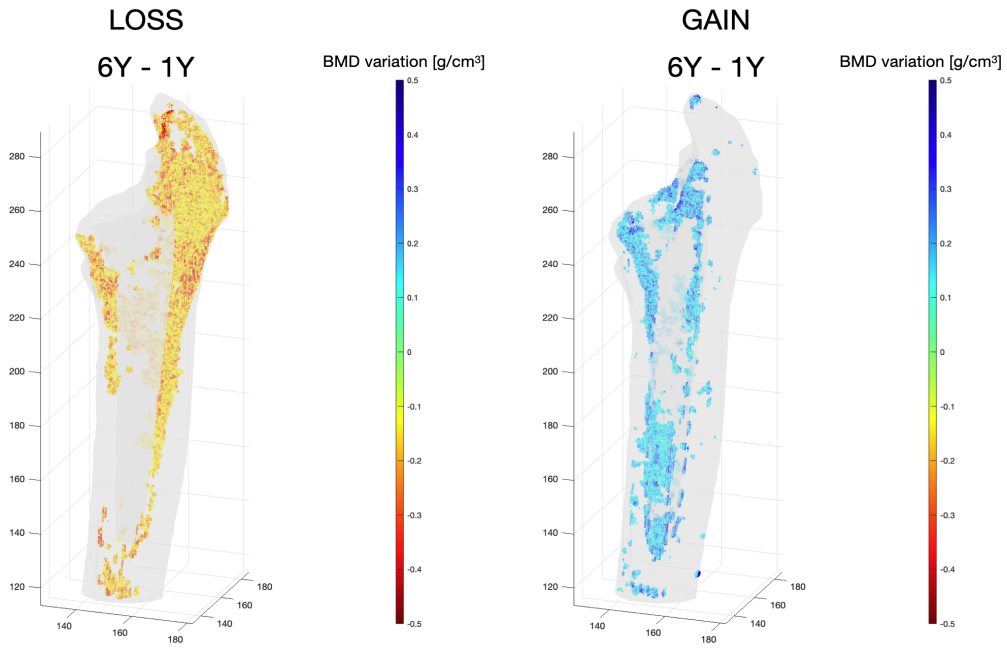

Figure 4.2: 3D BMD evaluation six years post-operation (female cemented). Blue points states for a gain, orange ones for a loss. The threshold was set at $\pm$ 0.1 g/cm^3.

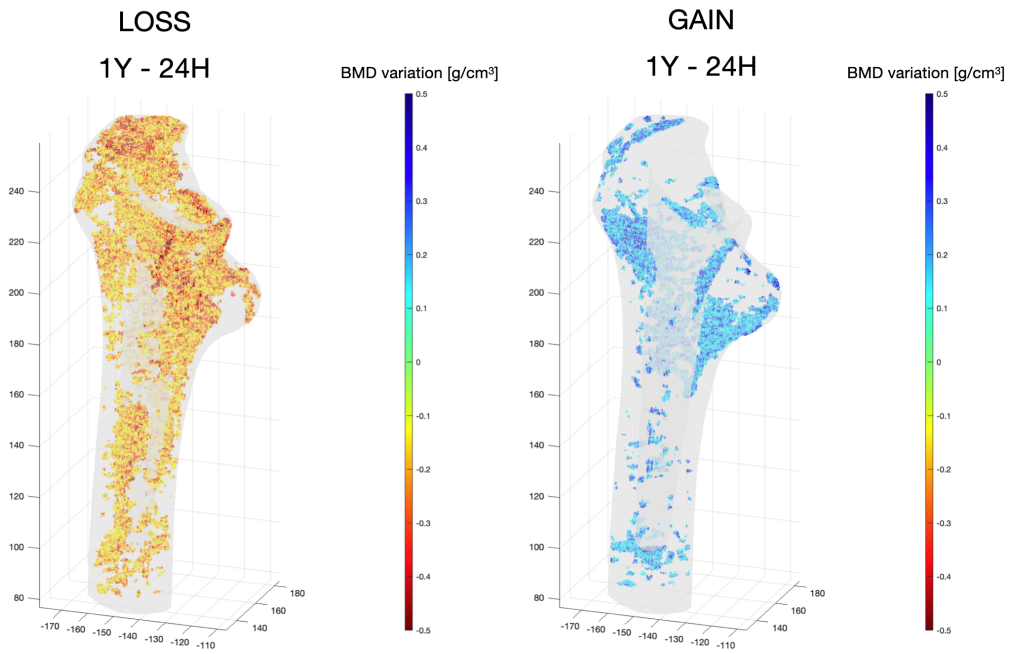

Figure 4.3: 3D BMD evaluation one year post-operation (male uncemented). Blue points states for a gain, orange ones for a loss. The threshold was set at $\pm$ 0.1 g/cm^3.

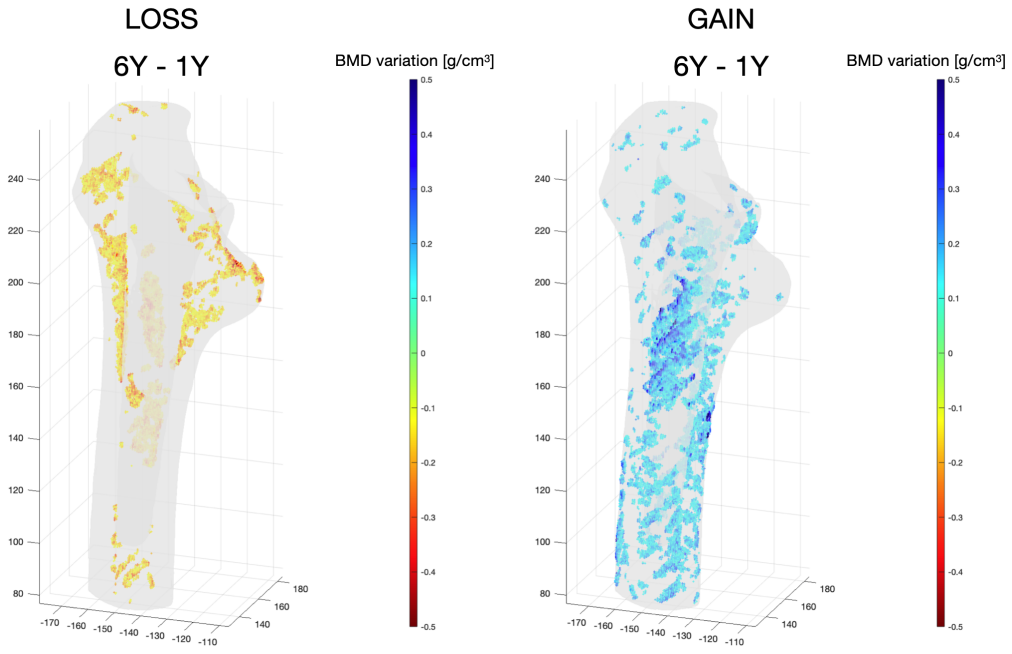

Figure 4.4: 3D BMD evaluation six years post-operation (male uncemented). Blue points states for a gain, orange ones for a loss. The threshold was set at $\pm$ 0.1 g/cm^3.

Limitations

Despite trying to minimise the intra- and inter-operator variability, the methodology presented in this work has its limitations that can affect the accuracy of BMD changes assessment.

First of all, two different CT machines were employed in this study, since the post 24h and post 1y data were acquired with a *Philips Brilliance 64 Spiral-CT* machine, while post 6y data with a *Toshiba Aquilion PRIME*. These two scanners have different specifications, as shown in tab. 2.2. Despite the uniformation of pixel sizes done with the reslicing tool, this factor would certainly introduce some uncertainties.

Another source of error is caused by the reslicing operation. Being a operator-dependent task, some differences between the alignment for different datasets can occur. However, this issue does not seem to have a large impact on the final result, differently to another operator-dependent task of the method. Indeed, the cutting plans used to split the femur masks to obtain the Gruen zones are hand selected by the operator. Despite the use of the measurement tools to assess the right point, this operation may lead to a certain error. To overcome this issue, an automatic algorithm is currently in development. Such tool will avoid standard-issues made by the intra- and inter-operator variability.

Another issue regards the choice of the range of values to perform bone segmentation, set from 250 HU to 2999 HU. In particular, the lower limit seems to be critical, since some of the patients may have spongeous bone with even lower HU values. This entails to the discarding of some pixels belonging to bone tissue. However, reducing the lower HU threshold leads to consider also soft tissue, that are undesirable for the purpose of this analysis. For this reason, that value was chosen as the best compromise among these two issues. Indeed, through the use of the "smart fill" tool, the majority of bone pixels discarded can be merged with the bone mask anyway.

Moreover, another important limitations relies on the limited number of subjects that have been undergo their post 6y CT-scan at the moment of this study. However, with the chance to assess a larger number of participants, it would be possible to draw conclusions on all these study questions.

Chapter 5

Conclusion and Future Developments

The *in silico* method presented in this work can be easily employed as a tool to assess the bone remodelling process occurring in the femur over the years. Indeed, it has been verified that the protocol is easily applicable to all the patients that underwent an unilater THA, and no discouragements are seen that could prevent the use of this method to assess BMD changes for subjects with a bilateral THA. As a result, any difference from these two different cohorts could be investigated. Certain general trends have been identified on this study cohort, wherein only ten patients were processed. However, through the addition of a larger amount of data, this methodology will provide a tool to draw conclusions regarding BMD changes over the years and where these variations are more precisely localised in the femur. Any correlation between age, sex, weight, level of physical activity pre- and post-operation, pre-existing diseases, drug therapies, as well as the type of the implant chosen and the surgical approach will be investigated.
Such analysis will be supplied to surgeons as a tool to develop new strategies not merely regarding the selection of the optimal implant, but also concerning the best approach to rehabilitation and adjoining pharmacological therapy.

References

[1] Elaine Marieb and Suzanne Keller. *Essentials of Human Anatomy & Physiology, 11th Edition*. Pearson, 2015. ISBN: 9781292057590.

[2] *The Hip Joint - Articulations - Movements - TeachMeAnatomy*. Library Catalog: teachmeanatomy.info. URL: https://teachmeanatomy.info/lower-limb/joints/hip-joint/ (visited on 10/21/2020).

[3] Maks Gold and Matthew Varacallo. *Anatomy, Bony Pelvis and Lower Limb, Hip Joint*. StatPearls Publishing, Treasure Island (FL), 2019. URL: http://europepmc.org/books/NBK470555.

[4] Basem Attum and Matthew Varacallo. *Anatomy, Bony Pelvis and Lower Limb, Thigh Muscles*. StatPearls Publishing, Treasure Island (FL), 2020. URL: http://europepmc.org/books/NBK482445.

[5] *WHO — Chronic rheumatic conditions*. Library Catalog: www.who.int Publisher: World Health Organization. URL: http://www.who.int/chp/topics/rheumatic/en/ (visited on 11/23/2020).

[6] Robert Pivec et al. "Hip arthroplasty". In: *The Lancet* 380.9855 (2012), pp. 1768–1777. ISSN: 0140-6736.

[7] Francesco Traina et al. *L'intervento di artroprotesi d'anca*. Sept. 2020.

[8] Agency for Healthcare Research and Quality. *Improving the Measurement of Surgical Site Infection Risk Stratification/Outcome Detection*. https://www.ahrq.gov/research/findings/final-reports/ssi/ssiexh19.html. (Visited on 11/22/2020).

[9] *Hip and knee replacement — Health at a Glance 2019 : OECD Indicators — OECD iLibrary*. en. Library Catalog: www.oecd-ilibrary.org. URL: https://www.oecd-ilibrary.org/sites/2fc83b9a-en/index.html?itemId=/content/component/2fc83b9a-en (visited on 12/27/2020).

[10] Progetto Registro Italiano ArtroProtesi. *Quarto Report 2017. Potenziare la qualità dei dati per migliorare la sicurezza dei pazienti*. http://riap.iss.it/riap/it/attivita/report/2017/12/15/quarto-report-2017/. (Visited on 12/22/2020).

[11] S. Birtwistle, K. Wilson, and M. Porter. "Long-term survival analysis of total hip replacement." In: *Annals of the Royal College of Surgeons of England* 78 3 (Pt 1) (1996), pp. 180–3.

[12] Ian Learmonth, Claire Young, and Cecil Rorabeck. "The operation of the century: Total hip replacement". In: *Lancet* 370 (Nov. 2007), pp. 1508–19. DOI: 10.1016/S0140-6736(07)60457-7.

[13] Amit Aherwar, Amit Singh, and Amar Patnaik. "Current and future biocompatibility aspects of biomaterials for hip prosthesis". In: *AIMS Journal* 3 (Jan. 2016), pp. 23–43. DOI: 10.3934/bioeng.2016.1.23.

[14] Ayham Darwich, Hasan Nazha, and William Abbas. "Numerical study of stress shielding evaluation of hip implant stems coated with composite (carbon/PEEK) and polymeric (PEEK) coating materials". In: *Biomedical Research* 30 (Feb. 2019), pp. 169–174. DOI: 10.35841/biomedicalresearch.30-18-1048.

[15] Yousuf Mahboba and Mohsin Al-Shammari. "Enhancing wear rate of high-density polyethylene (HDPE) by adding ceramic particles to propose an option for artificial hip joint liner". In: *IOP Conference Series: Materials Science and Engineering* 561 (Nov. 2019), p. 012071. DOI: 10.1088/1757-899X/561/1/012071.

[16] *Total Hip Replacement - OrthoInfo - AAOS*. Library Catalog: orthoinfo.aaos.org. URL: https://www.orthoinfo.org/en/treatment/total-hip-replacement/ (visited on 12/29/2020).

[17] Makarand Joshi et al. "Analysis of a femoral hip prosthesis designed to reduce stress shielding". In: *Journal of biomechanics* 33 (Jan. 2001), pp. 1655–62. DOI: 10.1016/S0021-9290(00)00110-X.

[18] Richard A Brand, John J Callaghan, and Richard C Johnston. "Total Hip Reconstruction". eng. In: *The Iowa Orthopaedic Journal* 11 (1991), pp. 19–42. ISSN: 1541-5457. URL: https://www.ncbi.nlm.nih.gov/pmc/articles/PMC2328971/.

[19] Stephen Richard Knight, Randeep Aujla, and Satya Prasad Biswas. "Total Hip Arthroplasty – over 100 years of operative history". In: *Orthopedic Reviews* 3.2 (Nov. 2011), e16. DOI: 10.4081/or.2011.e16. URL: https://www.pagepress.org/journals/index.php/or/article/view/or.2011.e16.

[20] European Commission. Joint Research Centre. Institute for Health and Consumer Protection. *Total hip arthroplasty: state of the art, challenges and prospects.* en. LU: Publications Office, 2012. URL: https://data.europa.eu/doi/10.2788/31286 (visited on 12/31/2020).

[21] Saverio Affatato. "Contemporary designs in total hip arthroplasty (THA)". In: *Perspectives in Total Hip Arthroplasty.* Ed. by Saverio Affatato. Woodhead Publishing, 2014, pp. 46–64. ISBN: 978-1-78242-031-6. DOI: https://doi.org/10.1533/9781782420392.1.46. URL: http://www.sciencedirect.com/science/article/pii/B9781782420316500040.

[22] Mike Reed et al. *National Joint Registry: 17th annual report (2020).* UK National Joint Registry, 2020.

[23] Kristine Bunyoz et al. "Has the Use of Fixation Techniques in THA Changed in This Decade? The Uncemented Paradox Revisited". In: *Clinical Orthopaedics and Related Research* 478 (Dec. 2019), p. 1. DOI: 10.1097/CORR.0000000000001117.

[24] Robert Pivec et al. "Hip arthroplasty". In: *Lancet (London, England)* 380.9855 (Nov. 2012), pp. 1768–1777. ISSN: 0140-6736. DOI: 10.1016/s0140-6736(12)60607-2. URL: https://doi.org/10.1016/S0140-6736(12)60607-2.

[25] Pablo Gomez and Jose Morcuende. "A Historical and Economic Perspective on Sir John Charnley, Chas F. Thackray Limited, and the Early Arthroplasty Industry". In: *The Iowa orthopaedic journal* 25 (Feb. 2005), pp. 30–7.

[26] M Halawa et al. “The shear strength of trabecular bone from the femur, and some factors affecting the shear strength of the cement-bone interface”. In: *Archives of orthopaedic and traumatic surgery. Archiv fur orthopadische und Unfall-Chirurgie* 92.1 (Aug. 1978), pp. 19–30. ISSN: 0344-8444. DOI: 10.1007/bf00381636. URL: https://doi.org/10.1007/bf00381636.

[27] *Sirius Cemented Femoral Hip Stem Surgical Technique*. en. URL: https://www.zimmerbiomet.com/content/dam/zimmer-biomet/medical-professionals/000-surgical-techniques/hip/sirius-cemented-femoral-hip-stem-surgical-technique.pdf (visited on 12/29/2020).

[28] Po-Liang Lai et al. “Hypothermic manipulation of bone cement can extend the handling time during vertebroplasty”. In: *BMC musculoskeletal disorders* 13 (Oct. 2012), p. 198. DOI: 10.1186/1471-2474-13-198.

[29] Joanna Maggs and Matthew Wilson. “The Relative Merits of Cemented and Uncemented Prostheses in Total Hip Arthroplasty”. In: *Indian Journal of Orthopaedics* 51 (July 2017), p. 377. DOI: 10.4103/ortho.IJOrtho_405_16.

[30] SD Cook, KA Thomas, and RJ Haddad. “Histologic analysis of retrieved human porous-coated total joint components”. In: *Clinical orthopaedics and related research* 234 (Sept. 1988), pp. 90–101. ISSN: 0009-921X. URL: http://europepmc.org/abstract/MED/3409607.

[31] K. Katti. “Biomaterials in total joint replacement.” In: *Colloids and surfaces. B, Biointerfaces* 39 3 (2004), pp. 133–42.

[32] *CORAIL® Hip System*. en. URL: https://www.corailpinnacle.net/sites/default/files/DSEMJRC061606652%5C%20CORAIL%5C%20Platform%5C%20Brochure.pdf (visited on 01/01/2021).

[33] Paolo Gargiulo et al. “Bone Mineral Density and Fracture risk assessment for patients undergoing total hip arthroplasty as support for decision making”. In: *European International Journal of Science and Technology (EIJST)* (June 2013).

[34] RL Wixson, SD Stulberg, and M Mehlhoff. "Total hip replacement with cemented, uncemented, and hybrid prostheses. A comparison of clinical and radiographic results at two to four years". In: *The Journal of bone and joint surgery. American volume* 73.2 (Feb. 1991), pp. 257–270. ISSN: 0021-9355. URL: http://europepmc.org/abstract/MED/1899667.

[35] Ali Abdulkarim et al. "Cemented versus uncemented fixation in total hip replacement: A systematic review and meta-analysis of randomized controlled trials". In: *Orthopedic reviews* 5 (Feb. 2013), e8. DOI: 10.4081/or.2013.e8.

[36] Kristoff Corten et al. "What Works Best, a Cemented or Cementless Primary Total Hip Arthroplasty?: Minimum 17-year Followup of a Randomized Controlled Trial". en. In: *Clinical Orthopaedics and Related Research®* 469.1 (Jan. 2011), pp. 209–217. ISSN: 1528-1132. DOI: 10.1007/s11999-010-1459-5. URL: https://doi.org/10.1007/s11999-010-1459-5 (visited on 01/02/2021).

[37] DD D'Lima et al. "100 cemented versus 100 noncemented stems with comparison of 25 matched pairs". In: *Clinical orthopaedics and related research* 348 (Mar. 1998), pp. 140–148. ISSN: 0009-921X. URL: http://europepmc.org/abstract/MED/9553546.

[38] Dale Sumner. "Long-term implant fixation and stress-shielding in total hip replacement". In: *Journal of biomechanics* 48 (Dec. 2014). DOI: 10.1016/j.jbiomech.2014.12.021.

[39] Marcus Streit et al. "Long-term (20-to 25-year) Results of an Uncemented Tapered Titanium Femoral Component and Factors Affecting Survivorship". In: *Clinical orthopaedics and related research* 471 (May 2013). DOI: 10.1007/s11999-013-3033-4.

[40] Thröstur Petursson et al. "Bone Mineral Density and Fracture Risk Assessment to Optimize Prosthesis Selection in Total Hip Replacement". In: *Computational and Mathematical Methods in Medicine* 2015 (Mar. 2015). DOI: 10.1155/2015/162481.

[41] Aliya Khan. "Premenopausal women and low bone density". In: *Canadian Family Physician* 52.6 (June 2006), pp. 743–747. ISSN: 0008-350X. URL:

https://www.ncbi.nlm.nih.gov/pmc/articles/PMC1780157/ (visited on 01/02/2021).

[42] Steven Kurtz et al. "Projections of Primary and Revision Hip and Knee Arthroplasty in the United States from 2005 to 2030". In: *The Journal of bone and joint surgery. American volume* 89 (Apr. 2007), pp. 780–5. DOI: 10.2106/JBJS.F.00222.

[43] H. Malchau, P. Herberts, and L. Ahnfelt. "Prognosis of total hip replacement in Sweden. Follow-up of 92,675 operations performed 1978-1990". eng. In: *Acta Orthopaedica Scandinavica* 64.5 (Oct. 1993), pp. 497–506. ISSN: 0001-6470. DOI: 10.3109/17453679308993679.

[44] Seung Lee et al. "Comparison Between Bipolar Hemiarthroplasty and THA for Osteonecrosis of the Femoral Head". In: *Clinical orthopaedics and related research* 424 (Aug. 2004), pp. 161–5. DOI: 10.1097/01.blo.0000128217.18356.87.

[45] A. D. Hanssen, D. R. Osmon, and C. L. Nelson. "Prevention of deep periprosthetic joint infection." English (US). In: *Instructional course lectures* 46 (1997), pp. 555–567. ISSN: 0065-6895.

[46] Maximillian Soong, Harry Rubash, and William Macaulay. "Dislocation After Total Hip Arthroplasty". In: *The Journal of the American Academy of Orthopaedic Surgeons* 12 (Sept. 2004), pp. 314–21. DOI: 10.5435/00124635-200409000-00006.

[47] R.W. Crawford and D.W. Murray. "Total hip replacement: indications for surgery and risk factors for failure". In: *Annals of the Rheumatic Diseases* 56.8 (1997), pp. 455–457. ISSN: 0003-4967. DOI: 10.1136/ard.56.8.455. eprint: https://ard.bmj.com/content/56/8/455.full.pdf. URL: https://ard.bmj.com/content/56/8/455.

[48] Subir Ghosh and Sylvester Abanteriba. "Status of surface modification techniques for artificial hip implants". In: *Science and Technology of Advanced Materials* 17 (Sept. 2016). DOI: 10.1080/14686996.2016.1240575.

[49] U. Hedlundh et al. “Surgical experience related to dislocations after total hip arthroplasty”. eng. In: *The Journal of Bone and Joint Surgery. British Volume* 78.2 (Mar. 1996), pp. 206–209. ISSN: 0301-620X.

[50] Massimiliano Merola and Saverio Affatato. “Materials for Hip Prostheses: A Review of Wear and Loading Considerations”. In: *Materials* 12 (Feb. 2019), p. 495. DOI: 10.3390/ma12030495.

[51] Juliet Compston. “Bone histomorphometry”. en. In: *Methods in Bone Biology*. Ed. by Timothy R. Arnett and Brian Henderson. Boston, MA: Springer US, 1998, pp. 177–197. ISBN: 978-0-585-38227-2. DOI: 10.1007/978-0-585-38227-2_7. URL: https://doi.org/10.1007/978-0-585-38227-2_7 (visited on 01/02/2021).

[52] David A. Bluemke and Songtao Liu. “Chapter 41 - Imaging in Clinical Trials”. In: *Principles and Practice of Clinical Research (Third Edition)*. Ed. by John I. Gallin and Frederick P. Ognibene. Third Edition. Boston: Academic Press, 2012, pp. 597–617. ISBN: 978-0-12-382167-6. DOI: https://doi.org/10.1016/B978-0-12-382167-6.00041-2. URL: http://www.sciencedirect.com/science/article/pii/B9780123821676000412.

[53] CF Njeh et al. “Radiation exposure in bone mineral density assessment”. In: *Applied radiation and isotopes : including data, instrumentation and methods for use in agriculture, industry and medicine* 50.1 (Jan. 1999), pp. 215–236. ISSN: 0969-8043. DOI: 10.1016/s0969-8043(98)00026-8. URL: https://doi.org/10.1016/s0969-8043(98)00026-8.

[54] Joseph Schreiber et al. “Hounsfield Units for Assessing Bone Mineral Density and Strength: A Tool for Osteoporosis Management”. In: *The Journal of bone and joint surgery. American volume* 93 (June 2011), pp. 1057–63. DOI: 10.2106/JBJS.J.00160.

[55] Giampiero I. Baroncelli. “Quantitative Ultrasound Methods to Assess Bone Mineral Status in Children: Technical Characteristics, Performance, and Clinical Application”. en. In: *Pediatric Research* 63.3 (Mar. 2008). Number: 3 Publisher: Nature Publishing Group, pp. 220–228. ISSN: 1530-0447.

DOI: 10.1203/PDR.0b013e318163a286. URL: https://www.nature.com/articles/pr200844 (visited on 01/04/2021).

[56] Hua Zhou, Shi Lu, and David Dempster. "Bone Remodeling: Cellular Activities in Bone". In: *Osteoporosis in Men* (Jan. 2010), pp. 15–24. DOI: 10.1016/B978-0-12-374602-3.00002-X.

[57] Meng-Xia Ji and Qi Yu. "Primary osteoporosis in postmenopausal women". In: *Chronic Diseases and Translational Medicine* 1 (Mar. 2015), pp. 9–13. DOI: 10.1016/j.cdtm.2015.02.006.

[58] Jeffrey Gimble et al. "Aging and Bone". In: Oct. 2009, pp. 19–33. ISBN: 978-1-84628-515-8. DOI: 10.1007/978-1-84628-697-1_2.

[59] Heikki Kröger et al. "Evaluation of periprosthetic bone using dual-energy X-ray absorptiometry: Precision of the method and effect of operation on bone mineral density". In: *Journal of Bone and Mineral Research* 11 (Oct. 2009), pp. 1526–1530. DOI: 10.1002/jbmr.5650111020.

[60] Christi J. Sychterz and Charles A. Engh. "The Influence of Clinical Factors on Periprosthetic Bone Remodeling". In: *Clinical Orthopaedics and Related Research®* 322 (1996). ISSN: 0009-921X. URL: https://journals.lww.com/clinorthop/Fulltext/1996/01000/The_Influence_of_Clinical_Factors_on.34.aspx.

[61] C.V. Albanese et al. "Bone Remodelling in THA: A Comparative DXA Scan Study between Conventional Implants and a New Stemless Femoral Component. A Preliminary Report". In: *HIP International* 16.3_suppl (2006). PMID: 19219815, pp. 9–15. DOI: 10.1177/112070000601603S03. URL: https://doi.org/10.1177/112070000601603S03.

[62] Takashi Nishii et al. "Longitudinal Evaluation of Time Related Bone Remodeling After Cementless Total Hip Arthroplasty". In: *Clinical Orthopaedics and Related Research®* 339 (1997). ISSN: 0009-921X. URL: https://journals.lww.com/clinorthop/Fulltext/1997/06000/Longitudinal_Evaluation_of_Time_Related_Bone.17.aspx.

[63] Bernd-Arno Behrens et al. “Influence of Hip Prosthesis Size and Its Coating Area on Bone Remodeling”. In: *IEEE Transactions on NanoBioscience* PP (Sept. 2017), pp. 1–1. DOI: 10.1109/TNB.2017.2750724.

[64] TA Gruen, GM McNeice, and HC Amstutz. “”Modes of failure” of cemented stem-type femoral components: a radiographic analysis of loosening”. In: *Clinical orthopaedics and related research* 141 (June 1979), pp. 17–27. ISSN: 0009-921X. URL: http://europepmc.org/abstract/MED/477100.

[65] C. A. Engh, C. Sychterz, and C. Engh. “Factors affecting femoral bone remodeling after cementless total hip arthroplasty”. eng. In: *The Journal of Arthroplasty* 14.5 (Aug. 1999), pp. 637–644. ISSN: 0883-5403. DOI: 10.1016/s0883-5403(99)90091-8.

[66] Jung Taek Kim and Jeong Joon Yoo. “Implant Design in Cementless Hip Arthroplasty”. In: *Hip & pelvis* 28.2 (June 2016), pp. 65–75. ISSN: 2287-3260. DOI: 10.5371/hp.2016.28.2.65. URL: https://europepmc.org/articles/PMC4972888.

[67] R Huiskes and David Nunamaker. “Local stresses and bone adaption around orthopedic implants”. In: *Calcified tissue international* 36 Suppl 1 (Feb. 1984), S110–7. DOI: 10.1007/BF02406143.

[68] Joseph Lovecchio. *Articular prostheses*. (class lecture, Biomaterials, Università di Bologna, Cesena, November, 2020).

[69] Andrea Menichetti. “In silico methods to evaluate Fracture Risk and Bone Mineral Density changes in patients undergoing Total Hip Replacement.” Tesi di Laurea Magistrale. Università degli Studi di Bologna, 2016.

[70] QRM. *Micro-CT HA Phantom for the calibration of CT-values*. https://www.qrm.de/en/products/micro-ct-ha-phantom/. (Visited on 02/23/2021).

[71] Dirk Wagenaar et al. “Quantitative Comparison of Commercial and Non-Commercial Metal Artifact Reduction Techniques in Computed Tomography”. In: *PLOS ONE* 10.6 (June 1, 2015). Ed. by Gayle E. Woloschak, e0127932. ISSN: 1932-6203. DOI: 10.1371/journal.pone.0127932. URL: https://dx.plos.org/10.1371/journal.pone.0127932 (visited on 02/06/2021).

[72] Benedikt Helgason et al. “Mathematical relationships between bone density and mechanical properties: a literature review”. In: *Clinical biomechanics (Bristol, Avon)* 23.2 (Feb. 2008), pp. 135–146. ISSN: 0268-0033. DOI: 10.1016/j.clinbiomech.2007.08.024. URL: https://doi.org/10.1016/j.clinbiomech.2007.08.024.

[73] Paolo Gargiulo et al. “Monitoring of muscle and bone recovery in spinal cord injury patients treated with electrical stimulation using three-dimensional imaging and segmentation techniques: methodological assessment”. In: *Artificial organs* (2011). ISSN: 1525-1594. DOI: 10.1111/j.1525-1594.2011.01214.x. URL: http://hdl.handle.net/2336/129274.

[74] M Pérez et al. “Validation of bone remodelling models applied to different bone tyoes using Mimics”. In: (Feb. 2021).

[75] Daren Lim Fat et al. “The Hounsfield value for cortical bone geometry in the proximal humerus—an in vitro study”. In: *Skeletal Radiology* 41.5 (May 2012), pp. 557–568. ISSN: 1432-2161. DOI: 10.1007/s00256-011-1255-7. URL: https://doi.org/10.1007/s00256-011-1255-7.

[76] Arild Aamodt et al. “Determination of Hounsfield value for CT-based design of custom femoral stems”. In: *The Journal of bone and joint surgery. British volume* 81 (Feb. 1999), pp. 143–7. DOI: 10.1302/0301-620X.81B1.8880.

[77] David Burr. “Cortical bone: a target for fracture prevention?” In: *Lancet* 375 (May 2010), pp. 1672–3. DOI: 10.1016/S0140-6736(10)60444-8.

[78] M Ito et al. “Contribution of trabecular and cortical components to the mechanical properties of bone and their regulating parameters”. In: *Bone* 31 (Sept. 2002), pp. 351–8. DOI: 10.1016/S8756-3282(02)00830-X.